Development of a Novel Biochar-Molecularly Imprinted Polymer Composite for Targeted Adsorption of Perfluoroalkyl Substances in Water Treatment Applications

Jessica Marie Steigerwald

A thesis

submitted in partial fulfillment of

the requirements for the degree of

Master of Science

University of Washington

2022

Committee:

Jessica Ray

Gregory Korshin

Program Authorized to Offer Degree:

Civil and Environmental Engineering

University of Washington

Abstract

Development of a Novel Biochar-Molecularly Imprinted Polymer Composite for Targeted Adsorption of Perfluoroalkyl Substances in Water Treatment Applications

Jessica Marie Steigerwald

Chair of the Supervisory Committee:
Jessica Ray
Civil and Environmental Engineering

Per- and polyfluoroalkyl substances (PFAS) are a class of emerging contaminants which have received considerable research and regulatory attention in the last decade because of their toxicity, persistence, and prevalence in environmental and human reservoirs. Adsorption by activated carbon is the current industry standard for PFAS removal during water treatment. Biochar materials produced from agricultural food waste have recently been explored as more sustainable, cost-effective alternatives to granular activated carbon for PFAS removal in water. For example, a novel spent coffee grounds biochar ("SCGKOH") produced and tested in this study possessed PFOS removal capabilities comparable to a commercially available activated carbon at environmentally relevant concentrations. SCGKOH demonstrated a maximum adsorption capacity of 43.4 mg/g compared to Filtrasorb® F300 activated carbon (55.7 mg/g) and a wood-based fly ash char (79.5 mg/g). PFOS adsorption by all materials increased in the presence of divalent cations but decreased when simulated effluent organic matter was added. This phenomenon has been observed in a number of studies which have shown that PFAS removal by biochar and activated carbon decreases significantly in matrices with high concentrations of organic matter or competing organic and inorganic species. Additionally, short chain PFAS compounds—which are replacing longer chain PFAS in some manufacturing

applications, and have shown many of the same toxic end points as their longer chain counterparts—are poorly removed by activated carbon and biochar. Thus, there is a need for a more selective PFAS removal method for water treatment. Molecularly imprinted polymers (MIPs) are a class of materials designed with high selectivity for a template compound used during synthesis to create an adsorption binding site with tailored size, shape, and affinity. MIPs have limited applications due to their small size which hinders deployment. In this study, the aforementioned SCGKOH biochar was modified with MIPs to facilitate targeted PFAS adsorption in water. Waste derived biochar presents a low cost, widely available, easily tunable, and high surface area substrate ideal for functionalization with a MIP coating. The biochar was first modified with amine groups via electrophilic aromatic substitution followed by reduction, or pyrolysis in the presence of melamine or ammonium chloride. Amine groups served as attachment points for MIP coating achieved via thermally activated radical initiated polymerization. A quaternary nitrogen-containing monomer was chosen to confer positive surface charge over a wide pH range – an important characteristic for effective PFAS adsorption. Materials were characterized using various physicochemical characterization techniques to confirm the success of each modification. PFAS adsorption capabilities were evaluated in the presence of simulated wastewater effluent organic matter, common ions, and co-occurring organics. Results indicated that the MIP coated biochar have higher selectivity for PFAS than the unmodified biochar with adsorption of PFOS > PFOA > PFBS. Regeneration of spent adsorbent was successfully achieved with a 70% methanol, 1% sodium chloride solution. These materials present a novel, cost-effective option for targeted removal of PFAS from wastewaters.

Acknowledgements

I would like to take this opportunity to thank my advisor, Jessica Ray, for providing me with the opportunity to conduct this research and for being an incredible mentor and role model. I would also like to acknowledge the members of my research group, in particular Fanny Okaikue-Woodi, Yuemei Ye, Jennifer Hooper, Daniela Soilis, and Shawnie Peng, this work would not have been possible without their help and friendship. Thank you as well to Dr. Martin Sadilek at the University of Washington Department of Chemistry Mass Spectrometry Facility for assistance and expertise with LC-MS/MS quantification and Dr. Samantha Young at the University of Washington Molecular Analysis Facility for assistance with X-Ray Photoelectron Spectroscopy data collection and analysis. Finally, I would like to thank my family and friends, in particular my parents Sheila and Joe Steigerwald, whose support and comic relief allowed me to continue my graduate school journey.

Contents

List of Figures

Figure A4. Percent removal of 91 ± 8 µg/L PFOS by 100 mg/L SCGKOH with and without calcium (26 mg/L) and magnesium (12 mg/L) ions in the presence and absence of 5 mM HEPES buffer.

Figure A5. Chemical structures of PFOS (A) and caffeine (B).

Figure A6. Kinetics modeling of PFOS adsorption rates onto (a) SCGKOH, (b) F300, and (c) MCG with the Langmuir-derived non-linear pseudo first order, linear pseudo first order, and linear pseudo second order models.

List of Tables

Chapter 1: Background and Motivation

Population increase, climate change impacts on precipitation patterns, and anthropogenic contamination of some freshwater sources has resulted in water scarcity around the globe.[1-3] One option for water scarce communities is to implement water reuse to alleviate some of the demand for new water resources through either direct or indirect potable reuse or non-potable reuse.[4,5] However, emerging contaminants (ECs) that remain following advanced water treatment present a challenge for water reuse.[6-8] In the case of potable reuse there may be drinking water regulations that mandate specific treatments for or maximum concentration levels of ECs.[4] Similarly, where wastewater effluent is diverted to non-potable reuse or environmental water bodies, the effluent may become a source of ECs to the environment. This diversion could negatively impact aquatic life and increase concentrations of ECs in downstream drinking water sources, and thus may be regulated under other frameworks like the National Pollutant Discharge Elimination System (NPDES) permit.[4,8]

Per- and polyfluoroalkyl substances (PFAS) are a class of emerging contaminants that have received considerable attention in recent decades because of their prevalence,[9-11] persistence,[11,12] treatment challenges,[7] and toxicity at low nanogram or microgram per liter concentrations.[13-15] Originally discovered in the 1930s,[16] PFAS have since been used in the United States and around the world for the manufacture of a range of products including non-stick and stain resistant coatings,[17] electronics manufacturing,[18] food packaging,[17] and firefighting foams.[17,19] The U.S. Environmental Protection Agency (US EPA) has identified a list of 9,252 distinct PFAS compounds,[20] however all of them have two identifying characteristics. A carbon chain that is either partially (poly) or fully (per) fluorinated and a charged head group that is often anionic but may be cationic or zwitterionic.[17,20] Two of the most common classes of PFAS are perfluoroalkyl

carboxylic acids (PFCAs) and perfluoroalkyl sulfonic acids (PFSAs) having a fully fluorinated, hydrophobic tail which can vary in length from one to more than ten carbons and a carboxylic or sulfonic head group, respectively, which confers a negative charge at most environmental pH.[17,20] This structure gives PFAS surfactant-like properties which allow them to transport long distances in the environment.[21] The strength of the fluorocarbon bond (one of the strongest bonds possible) also makes these compounds resistant to passive environmental or biological degradation.[17,21] More recently, PFAS compounds containing an ether linkage within the fluorocarbon tail have been developed for manufacturing use with the goal that the ether would provide a degradation route for these chemicals which would decrease their longevity in the environment.[11] Unfortunately, recent studies have shown these compounds often transform within the environment to shorter chain PFCAs[12,17] and share many of the same toxic end points with their long chain and non-ether containing counterparts.[13,14,22]

A number of negative health impacts have been linked to human exposure to PFAS including immunosuppression and induction of tumors in liver, thyroid, and mammary glands.[23] Two of the more commonly identified PFAS in environmental systems, perfluorooctanoate (PFOA) and perfluorooctanesulfonate (PFOS), have received considerable research attention because of their prevalence and toxicity.[13,24,25] PFOA has been classified as possibly carcinogenic to humans and evidence has been found for the carcinogenicity of PFOS in humans as well.[23,24,26] Three main routes of human exposure to PFAS are inhalation of PFAS-containing dust, and consumption of contaminated food or drinking water.[23] Studies in rats have shown oral routes of exposure result in a high fraction of absorption of over 95% and account for the greatest portion of chronic exposures.[23] Once it enters the body, PFAS can bind to albumin proteins allowing them to become widely distributed throughout the body with highest concentrations found in the liver,

kidneys, and blood serum.[23] PFAS may also be transferred from mother to fetus during pregnancy or to infants via breast milk.[26] Many of the toxic outcomes of PFAS exposure identified to date result from activation of PPARα, a peroxisome proliferator-activated receptor that is important for energy homeostasis and which regulates gene expression for fatty acid oxidation.[23,27] The structure of PFAS molecules allow them to mimic the fatty acid molecules that typically activate the PPAR alpha nuclear receptors.[26]

In the early 2000s, PFOS and PFOA began to be phased out of production and manufacturing processes in the U.S. and elsewhere around the world in response to findings concerning their toxicity.[23] By 2015 their use in manufacturing in the U.S. had been almost completely eliminated.[18] In 2009 the US EPA released guidance on a human health advisory limit (HAL) for PFOS and PFOA in drinking water.[28] This HAL was updated in 2016 when the recommended drinking water limits for PFOS and PFOA either separately or combined were reduced to 70 nanograms per liter (ng/L).[28]

An important non-point source of PFAS to environmental systems and drinking water sources is wastewater treatment plant (WWTP) effluent. Recent research has focused on quantifying the presence, types, and fate of PFAS in WWTP.[29-34] An EPA memorandum released in April 2021 recognized wastewater as a potentially important source of PFAS as well.[35] Studies have identified a range of long and short chain PFAS as well as various precursor compounds in WWTP influent and effluent streams with concentrations ranging from the low nanogram per liter to high microgram per liter.[29,30]A recent study by Thompson et al. noted a national trend of decreasing concentrations of long chain PFAS and a potential increase in concentrations of short chain PFAS in WWTP.[29] During wastewater treatment, a fraction of the PFAS partition to the suspended solids and end up in the biosolids stream while the rest remain in the aqueous phase and exit the plant in

the wastewater effluent stream.[29,30] Precursor compounds are often transformed to their PFAS counterparts through biological or abiotic processes, increasing the total PFAS load through the plant.[29,30] PFAS removal with activated carbon (AC), which is commonly employed in drinking water treatment, is typically not a good choice for wastewater treatment because (1) high organic matter concentrations in wastewater tend to reduce the effectiveness of AC for PFAS adsorption, and (2) short chain PFAS compounds are poorly removed by AC.[11,36] Thus, a more selective adsorbent is needed for these treatment applications.

Chapter 2: Adsorption Behavior of Perfluorooctanesulfonate (PFOS) onto Activated Spent Coffee Grounds Biochar in Synthetic Wastewater Effluent[37]

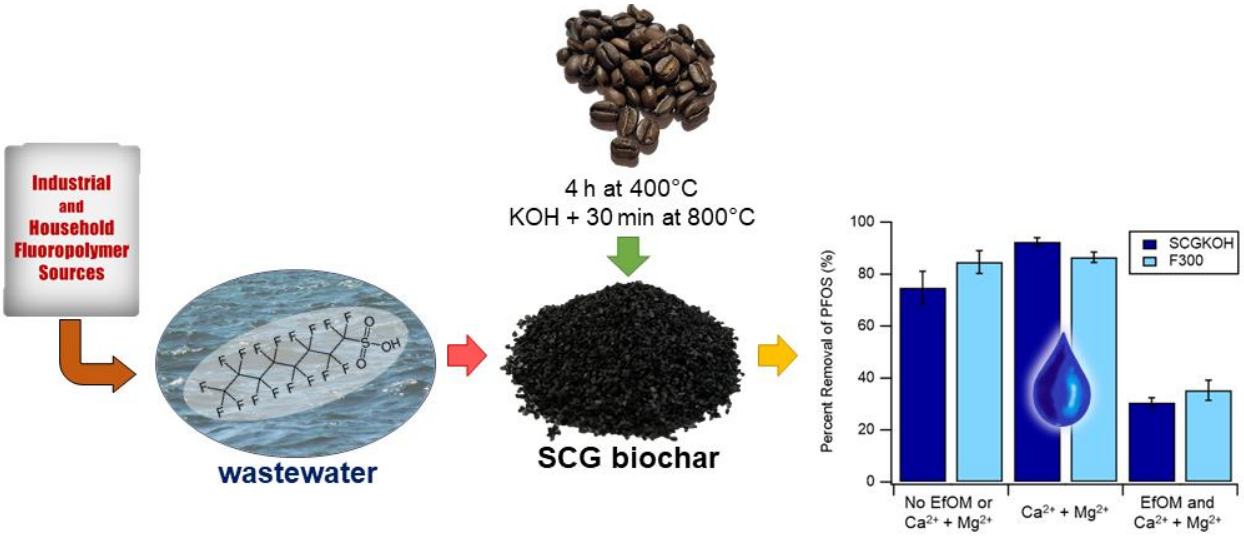

2.1 INTRODUCTION

Per- and polyfluoroalkyl substances (PFAS) are a class of surfactants with high thermal and structural stability used in aqueous film-forming foams for extinguishing hydrocarbon fires[19,28,38] and in the manufacture of many fluoropolymer end products.[28,38-41] PFAS chemical properties also promote their transport in air,[10] water,[9,10,12,21,33,34,42] sediments,[43] and biota[43] allowing these compounds to: (i) disperse in the environment,[21,33] (ii) resist degradation,[9,12,21,33,34,42] and (iii) present multiple exposure pathways to humans.[10,21,42]

Perfluorooctanesulfonate (PFOS) is a commonly detected PFAS in the environment.[32] Wastewater effluent is an important source of low-level environmental PFOS concentrations which is particularly concerning where direct or indirect potable water reuse is being considered.[30,31,44,45] Exposure to PFOS has been linked to potential for negative human developmental and reproductive effects (i.e., the basis for the Environmental Protection Agency (EPA) 70 ng/L health advisory limit and imminent regulatory limit), and has been shown to cause kidney, liver, and hematologic defects in rodents.[24,28,42] Recent guidance from regulatory agencies across the United States suggests even lower levels of PFOS (e.g., 10–15 ng/L) may present human health risks.[46-48]

PFAS adsorption using activated carbon (AC) is the most common approach to separate PFAS from water.[38,42] Commercial AC are traditionally produced from coal-based or coconut shell feedstocks via energy intensive pyrolysis, and activation with alkaline hydroxide or other more toxic chemicals.[42] Recently, biochar and activated biochar produced from carbonaceous agricultural food waste via less energy intensive methods have gained popularity as potentially more cost-effective and resource-efficient adsorbent alternatives for water treatment applications (e.g., in resource-constrained regions).[6,49] Char materials produced from spent coffee grounds

(SCG), an abundant food waste in many locales, is one such option. Potassium hydroxide (KOH) activation can be employed to oxidize the pyrolyzed char material, producing an activated char with low ash content, relatively uniform pore size distribution, and high contaminant removal capabilities.[50] For example, Deng et al. (2015) achieved 75% removal of 100 mg/L PFOS in 24 h with a KOH-activated bamboo biochar.[51] Activated SCG biochar has been employed for adsorption of several (in)organic contaminants (including phenol and dysprosium);[52-55] however, adsorption of PFAS with this material has not, to our knowledge, been investigated.

The focus of this study was to produce and characterize SCG biochar for PFOS adsorption.[50,52,53,56] Due to its environmental prevalence and ease of adsorption by activated char materials,[32] PFOS was an ideal PFAS adsorbate candidate to evaluate the competitiveness of our material with commercial options. The SCG biochar physicochemical properties and performance were compared to those of commercial activated carbon (Filtrasorb® 300) and a mixed softwood gasification biochar with demonstrated high PFAS adsorption.[19,57,58] The objectives of this study were threefold: (1) to identify optimal SCG biochar production and activation conditions, (2) to relate char physicochemical properties to PFOS adsorption, and (3) to investigate adsorption capacities and mechanisms as a function of PFOS concentration, equilibrium time, and solution composition.

2.2 MATERIALS AND METHODS

2.2.1 Biochar Production

Upon receipt, Calgon Carbon™ Filtrasorb® 300 (F300) and Mountain Crest Gardens (MCG) biochar were ground and sieved to a No. 30 (595 µm) to 50 (297 µm) mesh fractions, rinsed with deionized water until the rinse water was clear, and dried at 90 °C overnight in a VWR 1500E

incubator (VWR International, Radnor, PA). The SCG were obtained directly after use, and immediately dried at 90 °C for 42 hours and stored in an air-tight container to prevent molding.

Carbonization of the SCG was achieved using a Hogentogler Protégé Split Tube Furnace (Hogentogler, Colombia, MD). The material was heated to 200 °C at 10 °C/min and held there for 1 h to facilitate complete evaporation of trapped pore water. The material was then heated to 400 °C, 600 °C, or 800 °C at the same ramp rate and held at those temperatures for 4 h before cooling to produce the SCG400, SCG600, and SCG800 biochar, respectively. Nitrogen gas at 500 mL/min[53,54] flowed through the furnace during heating and cooling to maintain oxygen poor environments.

2.2.2 SCG Biochar Activation with Alkaline Hydroxide

Chemical activation of the SCG400 biochar was performed with sodium hydroxide (NaOH) and potassium hydroxide (KOH) to increase surface area and improve adsorption capabilities. SCG400 was selected as a precursor material because of its high yield of particles larger than 297 µm (24%), and relatively lower energy input compared to SCG600 and SCG800 biochar (23% and 21% yield). Briefly, SCG400 was thoroughly mixed with alkaline hydroxide pellets in a quartz crucible boat with SCG400:hydroxide mass ratios of 0.5, 1.0, 1.5, and 2.0. The boat was loaded in the tube furnace, and nitrogen gas flow (500 mL/min) was started and allowed to equilibrate prior to heating. The SCG400 was heated to 200 °C at 10 °C/min and held there for 1 h to evaporate residual water. The temperature was then increased to 800 °C at 10 °C/min and held there for 30 min to facilitate oxidation by the alkaline hydroxide.

Following activation, the media was first rinsed with a hydrochloric acid solution (0.002 – 0.01%) and then with deionized water until a 30-min equilibrium solution pH of 7.0 ± 0.5 was

achieved. The activated SCG biochar was then dried at 90 °C overnight, sieved to obtain the 297 – 595 µm size fraction, and stored in air-tight containers until further use.

2.2.3 Char Physicochemical Characterization

Proximate carbon analysis[59,60] of F300, MCG, SCG chars and feedstock, and CHN elemental analysis of the char media were conducted to provide a better understanding of their chemical composition differences. Caffeine release from the SCG char was evaluated to determine whether trapped caffeine in the SCG biochar could contaminate water sources during implementation. Specific surface area and pore size were evaluated via Brunauer-Emmett-Teller (BET) nitrogen adsorption at 77 K. Additional media characterization including scanning electron microscopy (SEM) imaging, surface zeta potential measurement, and diffuse reflectance infrared Fourier transform spectra (DRIFTS) analysis were completed to provide information about morphology, surface charge, and surface functional groups, respectively. Details on the methodology and results for these analyses are discussed in Appendix A: Supplementary Materials (App. A).

2.2.4 Batch Testing

All batch testing was done with the 297 – 595 µm char size fraction in 50-mL polypropylene centrifuge tubes with samples equilibrated via rotation at 40 rpm using a Fisherbrand™ Multi-Purpose Tube Rotator (Fisher Scientific, Waltham, MA). Preliminary evaluation of PFOS adsorption on the precursor was conducted and showed little PFOS

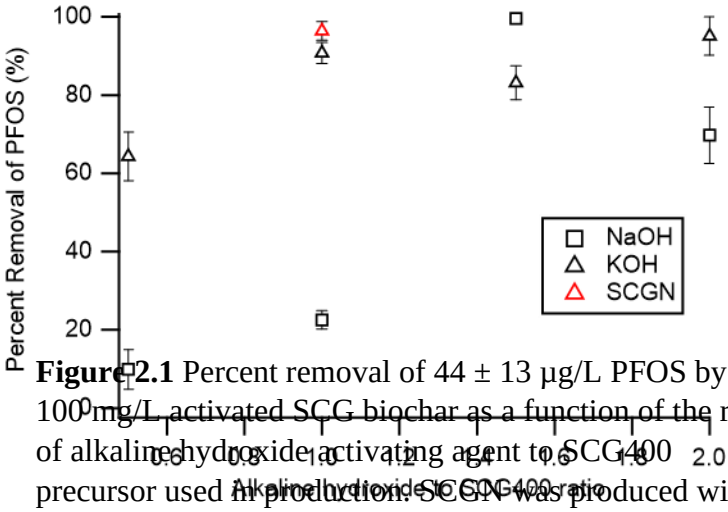

Figure 2.1 Percent removal of 44 ± 13 µg/L PFOS by 100 mg/L activated SCG biochar as a function of the ratio of alkaline hydroxide activating agent to SCG400 precursor used in production. SCGN was produced with the second batch of spent coffee grounds.

adsorption on any of the precursor materials (**Figure A3**). After SCG400 activation with various mass ratios of NaOH or KOH, 24-h batch adsorption tests were conducted with 100 mg/L char dose to evaluate their removal capabilities (**Figure 2.1**). Briefly, 5.0 mg of adsorbent was added to 50 mL of ultrapure water in 50-mL polypropylene centrifuge tubes and spiked with PFOS stock solution in methanol to obtain an initial PFOS concentration of 44 ± 13 µg/L. Samples were equilibrated for 24 h and filtered as described in App. A. The activated SCG400 biochar produced with 50 wt% KOH was selected for additional batch testing because of its good PFOS removal capabilities and comparatively low chemical input requirements. The activated SCG400 is henceforth identified as SCGKOH. Production and PFOS adsorption evaluation were repeated with a second SCGKOH material produced with a different batch of spent coffee grounds (SCGN; collected approximately 8 months after the first batch). Results show little difference in PFOS removal between SCGKOH batches, confirming the reproducibility of the pyrolysis and activation processes.

PFOS batch adsorption kinetics onto SCGKOH, F300, and MCG were evaluated over 5 days using triplicate, sacrificial samples for each time step. Approximately 5 mg of activated carbon was added to 50 mL of ultrapure water (Milli-Q systems, 18.2 MΩ-cm) and spiked with PFOS to obtain an initial PFOS concentration of 245 ± 20 µg/L. To control the solution pH and eliminate the effect of varying pH on PFOS adsorption,[61-63] a 4-(2-hydroxyethyl)piperazine-1-ethanesulfonic acid (HEPES) buffer was added at 5 mM, and the initial pH was adjusted to 7.0 ± 0.1 with 0.05 M NaOH. Samples were collected at various time points, filtered, and analyzed for PFOS adsorption as described in App. A. Kinetics data was fit to linear and non-linear pseudo first order, and linear pseudo second order kinetics models (calculations in App. A).

Batch adsorption isotherm tests were conducted with SCGKOH, F300, and MCG and fitted to the Langmuir and Freundlich isotherm models (calculations in App. A). Approximately 5 mg of activated carbon was added to 50 mL of ultrapure water and spiked with PFOS stock to obtain triplicate samples with initial PFOS concentrations between 2 and 8900 µg/L. HEPES buffer addition and pH adjustment were conducted as described above. Samples were equilibrated for 5 days before filtration and PFOS quantification.

Effects of representative divalent cations (i.e., 26 mg/L calcium as $CaCl_2$ and 12 mg/L magnesium as $MgCl_2$) in the presence and absence of simulated wastewater effluent organic matter (sEfOM) on PFOS removal by SCGKOH, F300, and MCG were evaluated with 24-h batch testing at an initial PFOS concentration of 340 ± 23 µg/L to inform evaluation of material performance for water treatment applications. Simulated effluent organic matter was synthesized as discussed by Motsa et al.[64] Briefly, four representative compounds, bovine serum albumin (2.5 mg/L), sodium alginate (2 mg/L), octanoic acid (0.5 mg/L), and humic acid (5 mg/L) were chosen to mimic the protein, carbohydrate, fat, and humic composition of typical EfOM.[64-67] Additional batch test experimental details, results of the SCG comparison test, analytical chemical information, and liquid chromatography tandem mass spectrometry (LC-MS/MS) procedures for PFOS and caffeine quantification are provided in App. A.

2.3 RESULTS AND DISCUSSION

2.3.1 Increased Surface Area Through Alkaline Activation

Physicochemical characterization of the SCG materials indicate carbonization (i.e., increased fixed carbon content via elimination of volatile carbon) predominantly occurred in the initial pyrolysis step while a dramatic increase in surface area occurred in the second activation step. The SCG feedstock had a low fixed carbon content (17.0%) and a high volatile carbon content (81.9%,

Table 2.1). After pyrolysis, the relative composition reversed with a fixed carbon content of 71.1% (SCG400) to 87.1% (SCG800) and a volatile carbon content of 25.2% (SCG400) to 7.9% (SCG800). The pyrolyzed SCG had low surface areas with the SCG400 having a surface area of 3 m^2/g prior to activation and 858 m^2/g after activation.

The char materials used for PFOS adsorption experiments displayed comparable elemental composition characterized by high fixed carbon content. For example, the SCGKOH fixed carbon (84.8%) and ash content (3.9%) were comparable to that of F300 (83.0% and 6.8%) and MCG (83.5% and 5.0%, **Table 2.1**). As expected, the proximate carbon results for F300 were similar to previously reported values[57] indicating minimal compositional change following grinding and washing processes. The SCGKOH displayed noticeably higher nitrogen content (2.17%) than either F300 (0.72%, reported elsewhere [57]) or MCG (< 0.005%), potentially indicating the presence of nitrogen-containing functional groups (e.g., $–NH_2$ moieties) which have been shown to contribute to contaminant adsorption.[68,69]

SCGKOH, F300 and MCG chars were characterized by high specific surface area and small average pore size (**Table 2.1** and **Table A2**), indicative of high adsorption capacity. Additionally, the char materials had a negative surface charge (**Table A3**) and limited identifiable DRIFTS surface functional groups (**Figure A2**). Both of these physicochemical properties are characteristic of materials with a high aromatic carbon content, which is suitable for hydrophobic interactions with the hydrophobic C–F PFOS backbone (chemical structure in **Figure A5**).[19,70]

2.3.2 Adsorption Kinetics Suggest Linear Driving Force

PFOS adsorption kinetics data were fit to pseudo first order (PFO) and pseudo second order (PSO) models (frequently used to describe liquid-to-solid adsorption) to obtain information about

the PFOS uptake rates and dynamic adsorption behavior.[71] The non-linear PFO model derived from the Langmuir kinetic model described by Liu and Shen (calculations in App. A)[72] provided

Table 2.1 Elemental composition and proximate carbon analysis of all SCG chars, F300 and MCG materials.

sample ID[1]	BET SA (m^2/g)	pore size[3] (nm)	elemental analysis[4,5]				proximate carbon analysis[5]		
			C %	H %	N %	O %[6]	VC %	FC %	Ash%
SCG	NA	NA	NA	NA	NA	NA	81.9 ± 0.3	17.0 ± 0.3	1.1 ± 0.0
SCG400	3	–	75.11 ± 0.55	4.24 ± 0.14	4.16 ± 0.05	12.76	25.2 ± 0.4	71.1 ± 0.4	3.7 ± 0.0
SCG600	7	–	79.56 ± 0.37	1.84 ± 0.08	3.86 ± 0.03	10.62	12.0 ± 0.5	83.7 ± 0.3	4.3 ± 0.2
SCG800	13	45.55	79.12 ± 0.79	1.15 ± 0.06	3.73 ± 0.22	11.35	7.9 ± 0.2	87.1 ± 0.1	5.0 ± 0.2
SCGKOH	858	1.42	81.42 ± 2.26	0.76 ± 0.02	2.17 ± 0.06	12.23	11.4 ± 0.7	84.8 ± 0.6	3.9 ± 0.2
F300[2]	1060	2.45	87.37[2]	0.17[2]	0.72[2]	4.59[2]	5.0	83.0	6.8
MCG	801	2.21	81.33 ± 0.31	1.21 ± 0.05	ND	12.82	11.5 ± 0.2	83.5 ± 0.3	5.0 ± 0.5

1. Samples were 297 – 595 µm size fraction.

2. F300 elemental analysis data from the Ulrich et al. (2015).

3. BJH average pore radius

4. Elemental analysis conducted on a wet-mass basis.

5. Values are the average of triplicate samples plus or minus the 95% confidence interval (with the exception of F300).

6. Oxygen composition calculated as 100% minus C, H, N, ash contributions.

SA – surface area; NA – not analyzed; ND – not detected, detection limit was 0.005%; VC – volatile carbon; FC – fixed carbon

a better fit for all three char materials than the linear PFO and linear PSO models (**Figure A6**). Application of the PFO model suggests PFOS adsorption is best described by a linear driving force; while the better fit of the non-linearized model corroborates previous findings that the log transformation required for PFO model linearization decreases the model's ability to accurately predict adsorption processes.[73,74] The SCGKOH, F300, and MCG chars showed fast initial PFOS uptake rates with over 70% PFOS removal within 24 h (**Figure 2.2, A1-C1**). The MCG in particular exhibited rapid adsorption kinetics ($k_{1,\,MCG}$ = 0.414 h^{-1}) with the majority of adsorption occurring within the first 6 h and equilibrium attained within 24 h. The long pores within MCG (**Figure 2.2, C1**) may contribute to this by providing shorter diffusion distances for PFOS molecules to inner pore spaces. The SCGKOH and F300 possessed slower initial adsorption rates ($k_{1,\,SCGKOH}$ = 0.062 h^{-1} and $k_{1,\,F300}$ = 0.090 h^{-1}), both reaching equilibrium around 48 hours and having a more uniform uptake rate throughout the initial 48 hours. This similarity in PFOS removal rates suggests SCGKOH is a promising candidate to replace commercial activated carbon during water treatment where adsorption time is often constrained by operational parameters.

2.3.3 Monolayer and Heterogeneous Binding of PFOS on Chars

Langmuir and Freundlich isotherm models fit to SCGKOH, F300, and MCG PFOS adsorption data suggest adsorption was characterized by both monolayer adsorption to homogeneous binding sites[75] (i.e., more dominant mechanism) and multilayer adsorption to heterogeneous binding sites (**Figure 2.2, A2-C2**; model description in App. A). SCGKOH, F300, and MCG exhibited correlation coefficients (R^2) greater than 0.9 for both isotherm models (**Figure 2.2 table**). Visual inspection of the data indicates adsorption on SCGKOH and F300 more closely follow a monolayer (Langmuir) scheme—particularly for data points at higher equilibrium PFOS

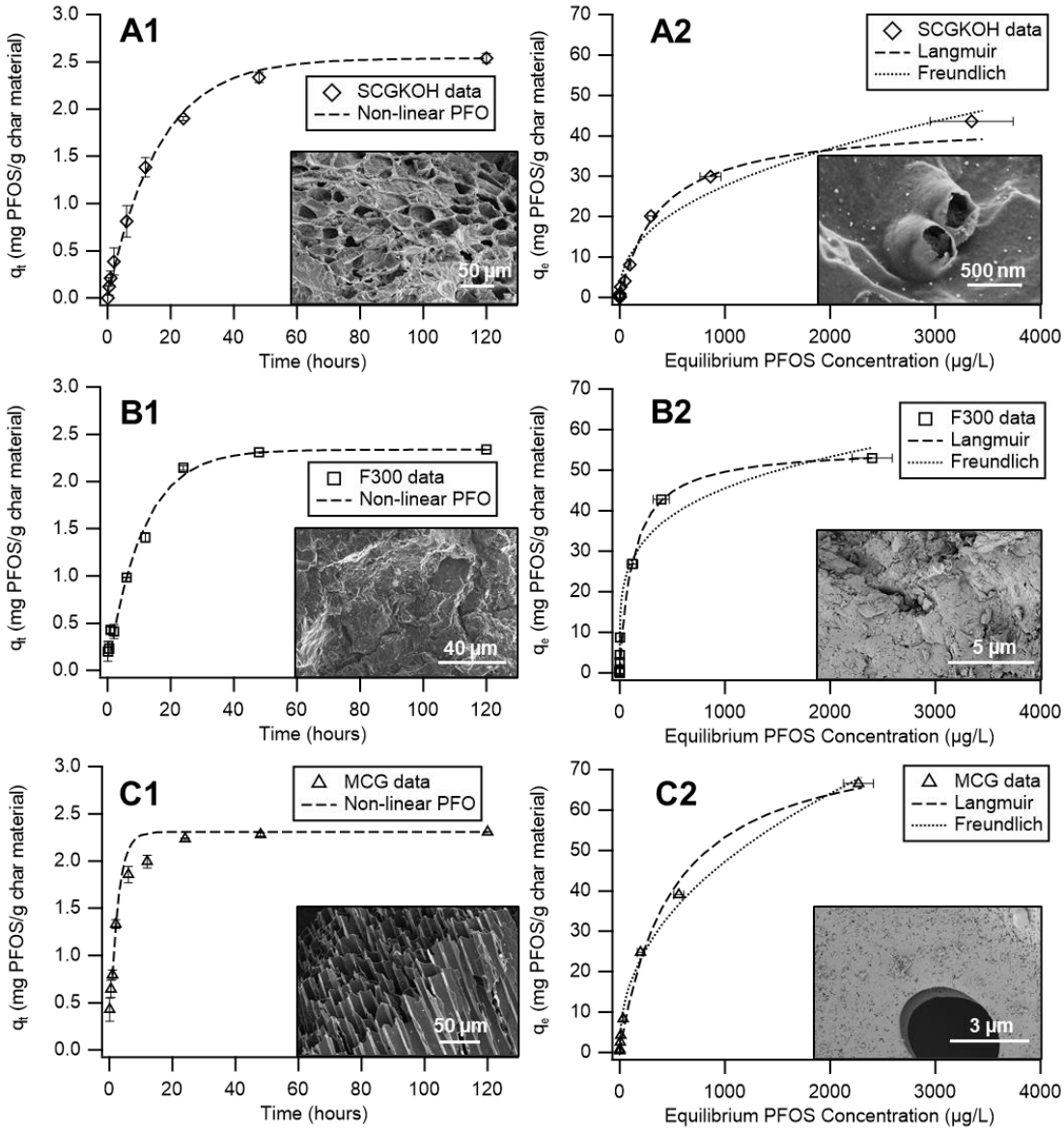

char material	non-linear pseudo first order		Langmuir			Freundlich		
	k_1 [h^{-1}]	σ^2	q_{max}	K_L	R^2	K_F	1/n	R^2
SCGKOH	0.069	0.003	43.4	0.003	0.996	1.581	0.414	0.988
F300	0.090	0.016	55.7	0.008	0.993	9.434	0.228	0.992
MCG	0.414	0.040	79.5	0.002	0.997	2.272	0.439	0.998

Figure 2.2 (1) Batch kinetics results of 245 ± 20 µg/L PFOS adsorption onto 100 mg/L (A) SCGKOH, (B) F300 and (C) MCG fit to the Langmuir kinetics-derived non-linear pseudo first order model with low magnification SEM image insets. (2) Isotherm PFOS adsorption data after a 5-d equilibrium fit to Langmuir and Freundlich models with high magnification SEM image insets. Error bars represent standard deviation of triplicate samples. Non-linear pseudo first order rate constant (k_1) and square error (σ^2), Langmuir maximum adsorption capacity (q_{max}) and adsorption rate constant (K_L), and Freundlich adsorption rate constant (K_F) and coefficient of non-linearity ($1/n$) are provided in the adjoining table.

concentrations—while the MCG adsorption data is equally well described by the Langmuir and Freundlich model, which denotes multilayer adsorption to sites with heterogeneous affinities for PFOS.[75] The heterogeneity of MCG adsorption sites could account for its more rapid PFOS uptake compared to SCGKOH and F300.

The Freundlich n^{-1} coefficient also indicate a degree of adsorption site non-linearity (n^{-1} = 0.414, 0.228, 0.439 for the SCGKOH, F300, and MCG, respectively; **Figure 2.2 table**) which may be due to multilayer adsorption or variability in adsorption site binding affinity. Some multilayer adsorption is likely due to PFOS-PFOS hydrophobic interactions[51,76] and hemimicelle formation either in solution or on the adsorbent surface,[77] particularly at high PFOS concentrations. Additionally, differences in binding affinity may be due to decreased time required for PFOS diffusion within the larger pores and surface features (**Figure 2.2, C1**).[73]

Interestingly, surface area alone was not a good predictor of adsorption capability for the three high surface area, high PFOS-adsorbing char materials. For example, MCG exhibited the lowest surface area but the greatest PFOS adsorption. Langmuir isotherm model parameter fitting for all three chars indicate MCG had the greatest PFOS adsorption capacity (79.5 mg PFOS/g char material) followed by F300 (55.7 mg/g) and then SCGKOH (43.4 mg/g). It is important to note that the inactivated SCG biochar possessing very low surface area also exhibit negligible PFOS adsorption (App. A), which suggests low surface area (i.e., 3–13 m^2/g) will decrease adsorption efficacy for chars. Zhi and Liu noted similar findings for PFOS adsorption onto various carbonaceous sorbents.[73] Furthermore, they suggested that point of zero charge (PZC) and adsorbent basicity (evaluated with Boehm titration) were better indicators of adsorption capability, and materials with high PZC and basicity will exhibit greater PFOS adsorption. Zeta potential results (**Table A3**) indicate a similar hypothesis may apply to the chars examined in this study as

the SCGKOH possesses the most negative zeta potential (-52.0 mV) followed by MCG (-26.2 mV) and F300 (-21.5 mV) under similar conditions. Evaluation of the PZC, surface acidity and basicity of these materials could provide a better understanding of the observed differences in PFOS adsorption capabilities.

2.3.4 Divalent Cations Improve and Hydrophobic sEfOM Inhibits PFOS Adsorption

Batch adsorption tests with divalent cations common in wastewater (26 mg/L Ca^{2+}, and 12 mg/L Mg^{2+}) showed an increase in PFOS removal capability for all three chars (**Figure 2.3**). In the presence of divalent cations alone, SCGKOH exhibited a 24% increase in PFOS adsorption from that exhibited in the calcium and magnesium free matrix (i.e., from 87.8% to 92.4%) while F300 and MCG each exhibited a 2% increase in PFOS removal (i.e., F300 from 84.7% to 86.5%; MCG from 93.3% to 95.3%). The presence of Ca^{2+} and Mg^{2+} has been observed elsewhere [78] to increase PFOS adsorption via ion bridging between the negatively charged char surface and the PFOS anionic headgroup. This mechanism is assumed to be principally responsible for the improved PFOS adsorption by SCGKOH as this adsorbent has the highest negative surface

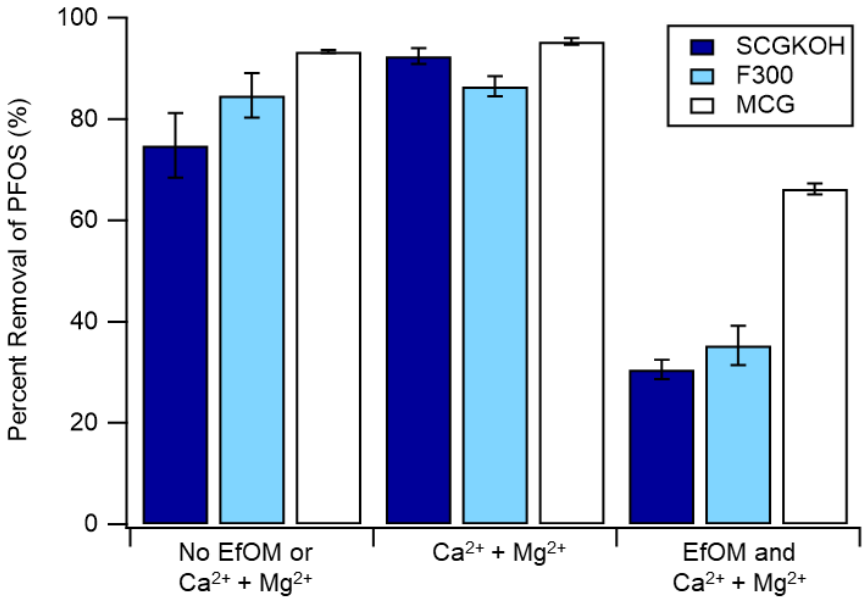

Figure 2.3 The effect of 10 mg/L simulated wastewater treatment plant EfOM, 26 mg/L Ca^{2+}, and 12 mg/L Mg^{2+} ions on 340 ± 23 µg/L PFOS removal by 100 mg/L SCGKOH, F300, and MCG.

charge: -52.0 mV (SCGKOH) compared to -26.2 mV (MCG) and -21.5 mV (F300) under similar conditions (**Table A3**).

By contrast, batch adsorption tests where representative wastewater effluent organic matter (10 mg/L sEfOM) was included in addition to divalent cations showed a significant reduction in PFOS removal for all media (**Figure 2.3**). The SCGKOH and F300 both experienced a 60% reduction in PFOS adsorption compared to the removal in the absence of sEfOM and divalent cations (i.e., SCGKOH from 74.8% to 33.6%; F300 from 84.7% to 35.3%). MCG was least impacted with only 29% decrease in PFOS removal (i.e., from 93.3% to 66.2%). The greater MCG PFOS removal can be partially attributed to its faster uptake kinetics which allowed for the equilibrium adsorption capacity to be achieved at a faster rate. Even given this difference in uptake rates, it appears MCG is the most effective char in more complex water matrices. The decrease in PFOS removal in the presence of sEfOM was assumed to be largely due to competition between hydrophobic sEfOM and PFOS for binding sites on the char materials, and surface passivation by sEfOM.[36] Importantly, the positive effect of ion bridging by divalent cations is masked in the combined studies by the competitive adsorption of co-occurring sEfOM. Further evaluation of adsorption behavior in matrices with increasing complexity could help elucidate these mechanisms.

2.4 CONCLUSIONS

Spent coffee grounds (SCG) are a widely available waste product and an ideal carbonaceous feedstock for low-cost biochar adsorbents. Initial pyrolysis of SCG produced a biochar with high carbon content, low surface area, and poor PFOS removal capabilities. Activation of this material with 50 wt% KOH resulted in more than 300-fold increase in surface area, yielding a char with PFOS removal capabilities comparable to Calgon F300 activated carbon and a wood-based biochar material with demonstrated efficacy in PFAS adsorption. Our isotherm results indicate that low

µg/L PFOS concentrations found in wastewater effluent would be treated to below the EPA PFOS HAL (i.e., 70 ng/L) using the SCGKOH. Introduction of simulated wastewater EfOM decreased PFOS removal on all three char materials. However, dissolved organic matter concentrations in drinking water are expected to be much lower; therefore, drinking water treatment using SCGKOH could be a viable application. Furthermore, the high PFOS removal exhibited by SCGKOH in the presence of divalent cations indicate this material will perform well in applications with moderate to high hardness but low organic content, such as drinking water treatment. The promising PFOS removal capabilities, abundant and low-cost waste-derived feedstock, and relatively low-resource production process make this material an advantageous option for water treatment in rural or resource-constrained areas. Future evaluation of short chain PFAS removal capability and options for spent adsorbent regeneration will improve our understanding of its capabilities for water treatment in varied systems. The size, structural integrity, and increased surface functional group heterogeneity of the SCGKOH can also facilitate further modification to improve adsorption capabilities for PFOS or other contaminants during water treatment.

Chapter 3: Immobilization of a PFOS-imprinted Polymer Coating on Coffee Grounds Biochar for Selective Removal of PFAS from Water[79]

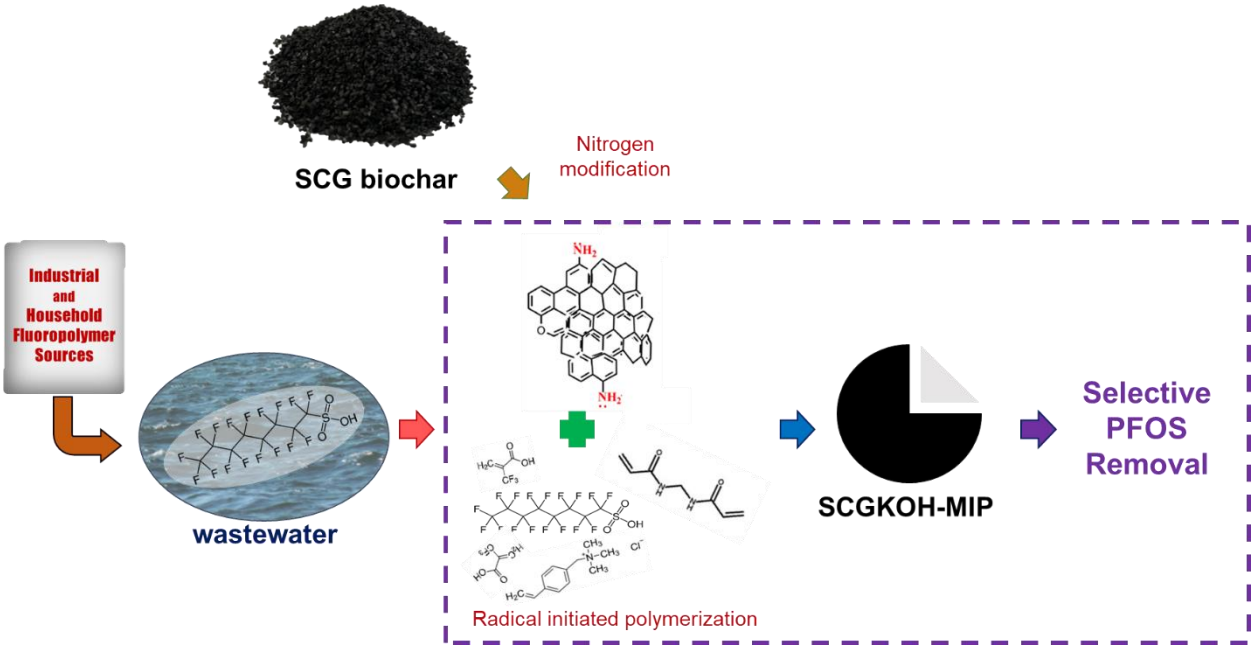

3.1 INTRODUCTION

Per- and polyfluoroalkyl substances (PFAS) are a class of chemicals which have been drawing increasing attention and concern in recent decades due to their prevalence,[9-11] persistence,[11,12] and negative human health impacts.[13-15] Originally developed in the 1940s for use in the manufacture of non-stick coatings and polymers,[17,80] PFAS use has expanded to a wide range of products including firefighting foams,[17,19] stain and water-resistant coatings,[17] food packaging,[17] and more. However, the unique synthetic design and physicochemical properties of PFAS (i.e., surfactant-like structure with hydrophilic head and hydrophobic tail)[21,33] also allow them to easily transport far distances in the environment and resist degradation (i.e., strong C-F bond),[9,42] resulting in an accumulation of PFAS in the environment.[9,40,78] In 2009, recognition of the potential human health impacts of PFAS exposure, even at very low levels, caused the U.S. Environmental Protection Agency (US EPA) to release a provisional drinking water health advisory limit (HAL) for two of the more common and toxic PFAS: perfluorooctanesulfonate (PFOS) and perfluorooctanoic acid (PFOA).[28] In 2016 the US EPA updated the HAL to 70 ng/L for PFOS and PFOA either individually or combined, and a maximum contaminant level (MCL) is currently being developed which is expected to be even lower than the existing HAL.[28,80] Regulation of PFOS, PFOA and other PFAS by the US EPA and other agencies – including upcoming MCLs anticipated for several PFAS – has prompted a shift in manufacturing toward use of shorter chain and polyfluorinated PFAS which were initially thought to be less toxic and less persistent in the environment.[11] However, recent research has shown that many polyfluorinated compounds transform in the environment to shorter chain perfluorocarboxylic acids (PFCAs),[17] and that these short chain PFAS share many of the same negative health outcomes with their longer chain counterparts.[13,14,22] Consumption of contaminated drinking water has been identified as one

of the dominant PFAS exposure route for humans.[81] Thus, there is a critical need for identification of efficient strategies for drinking water treatment and control of routes for PFAS contamination of drinking water sources.

An important non-point source of PFAS to environmental waters and drinking water sources that has received increased attention in recent years is wastewater treatment plant (WWTP) effluent.[10,29-31,80] PFAS may enter sewage through household sources, industrial discharges,[80] or landfill leachate[82,83] and are then removed poorly, if at all, by conventional wastewater treatment processes.[29] Wastewater effluent and biosolids containing PFAS compounds may then introduce PFAS to the environment where they disperse or may become a source of PFAS contamination for downstream drinking water sources. This is a particularly important consideration for areas where water reuse is being implemented or considered, such as in water constrained areas of the American (South)west.[45]

A key challenge associated with removal of PFAS from WWTP effluent relates to the lack of selectivity of current treatment options. The industry standard for removal of PFAS from drinking water (and groundwater where applicable) is adsorption onto a activated carbon (AC) media.[7,51,84] AC is a highly porous, pyrolyzed carbonaceous material characterized by its high specific surface area which allows it to readily adsorb a wide variety of organic and inorganic pollutants.[57,85] In WWTP effluent or groundwaters containing high dissolved organics or salt concentrations, competition for AC active sites arises between PFAS and other adsorbate molecules leading to low PFAS removal rates[36]—particularly for shorter chain PFAS compounds.[11] Wastewater typically contains around 10 mg/L of total organic carbon (TOC)[65,67] and around 200 - 1000 mg/L of total dissolved solids (TDS; i.e., salts)[86] and much lower concentrations of PFAS (0.01 ng/L – 50 μg/L)[29,30] and other trace organic contaminants (0.01 – 20

μg/L).[65,87] This challenge was highlighted in chapter 2 which described the development of a sustainably sourced and cost effective activated biochar which exhibited high PFAS removal comparable to a commercially available AC in the absence of other organics but experienced a significant decrease in PFAS removal – again similar to that seen for the AC – when synthetic effluent organic matter (sEfOM) was included.[37] Pretreatment to remove dissolved organics and salts is often employed for groundwater systems, however, this is an expensive option and likely impractical for the majority of WWTP.

Additionally, a safe and reliable disposal method for spent AC containing PFAS has yet to be identified. Current practices typically resort to either landfill disposal or incineration,[18] both of which present environmental hazards. In landfills, PFAS from spent AC will predominantly partition to the aqueous phase and be removed with the landfill leachate which is often taken to a WWTP for treatment where the PFAS will either be re-adsorbed in AC filters or released to the environment.[83] During incineration PFAS are burned off to regenerate the AC, a process which is expected to release harmful fluorocarbons to the atmosphere.[88]

Molecularly imprinted polymers (MIP), a class of polymer materials traditionally used for sensing compounds,[89,90] present an exciting potential alternative adsorbent for PFAS treatment. The target molecule (i.e., the PFAS adsorbate) is used as a template during the assembly of the polymer to create an active site with size, shape, and affinity specifically tailored to the target molecule.[89-91] Functional monomers are often selected for specific moieties (e.g., quaternary nitrogen or fluorocarbon) or properties (e.g., hydrophobicity or hydrophilicity) that will enhance the affinity for the template. These characteristics make the MIP material highly selective for the template compound, even in the presence of compounds with similar structure or charge, making it an ideal candidate for use as a sensor or adsorbent for compounds present at low concentrations

in complex matrices (e.g., PFAS removal in wastewater effluent). After production, the MIP is rinsed with a regeneration solution to remove the target molecule and is then ready for use as a sensor or adsorbent. This same process can be leveraged to regenerate spent media to create a concentrated PFAS solution from which PFAS could be extracted either for reuse in manufacturing processes or for subsequent disposal. Prior research has demonstrated the effectiveness of MIP materials containing charged nitrogen and fluorocarbon moieties as PFAS sensors with detection limits in the low nanograms per liter range[90,92,93] and as adsorbent media with adsorption capacity up to 76 mg/g.[91] For example, Guo et al. developed a PFOS-MIP coated carbon microsphere using [2-(Methacryloyloxy)ethyl] trimethylammonium chloride and 2-(trifluoromethyl)acrylic acid as functional monomers and observed 29.7% removal of 50 μmol/L PFOS in the presence of other PFAS and competing organics.[91] While MIPs have been demonstrated to possess high selectivity and high affinity for templated PFAS, the material produced is typically a fine powder substance which limits use as adsorbent media during traditional water filtration applications. To resolve this obstacle to deployment, several studies have fixed MIPs onto structural frameworks such as silica particles, carbon and titanium oxide nano tube arrays, and carbon microspheres.[91,94-96]

Biochar materials have several key advantages that make them an ideal substrate for MIP coating. First, the waste feedstocks (e.g., spent coffee grounds) from which they are often produced have the advantage of being relatively low cost and widely available compared to many other substrate options.[97,98] Second, the high specific surface area and density of micropores characteristic of activated carbons and biochar—which has been shown to be a significant contributor to the success of these materials as adsorbents[99]—is expected to be retained during the MIP coating and aid in their water treatment capabilities. Third, biochar materials contain a high density of surface functional groups and are easily modifiable to add or alter functional groups via

well-established processes. In MIP coating applications, these functional groups can act as potential receptor sites where crosslinking of the substrate to the MIP may occur.[91] In particular, surface functional groups containing an N–H bond are expected to be able to participate in radical initiated polymerization, since these bonds have been shown to form radicals upon interaction with initiator compounds like 2,2-azobisisobutyronitrile.[100,101]

In this study, a MIP material assembled with PFOS as a target molecule was coated onto a spent coffee grounds activated biochar investigated previously[37] to produce a novel adsorbent composite with high PFAS selectivity. The objective of this work was threefold: (1) to modify the spent coffee grounds biochar with nitrogen containing functional groups via low-impact methods that do not significantly impact the biochar structure or PFAS removal capability; (2) successfully coat the nitrogen-modified biochar with a PFAS selective MIP layer; and, (3) evaluate the ability of the MIP-coated biochar to selectively remove and recover PFAS of varying chain length and head group in both pure water and a complex matrix more representative of WWTP effluent. Prior works have established the high potential of MIP materials for selective removal of PFAS from aqueous systems. To our knowledge, however, coating of MIP on a biochar substrate has yet to be explored. The similarities in size and shape between the novel MIP-coated biochar materials described herein and activated carbons commonly used in water treatment are expected to provide a distinct advantage for their deployment in existing treatment infrastructure.

3.2 MATERIALS AND METHODS

3.2.1 Biochar Production

Spent coffee grounds biochar was produced from locally sourced waste material via a two-step process: pyrolysis followed by activation. This process is described in detail chapter 2 and the associated publication.[37] Briefly, the feedstock was sourced from Bay Laurel Catering from

industrial scale drip coffee using Starbucks® Pike's Place™ roast and was immediately dried at 90°C for 42 hours and stored in a sealed container to prevent degradation and microbial growth. Carbonization of the spent coffee grounds was performed at 400°C for 4 hours in a Hogentogler Protégé Split Tube Furnace (Hogentogler, Colombia, MD) under a nitrogen atmosphere (nitrogen flow rate of 500 mL/min). Activation was achieved through mixing equal mass of the pyrolyzed material with potassium hydroxide (KOH) pellets followed by heating at 800°C for 30 minutes under a nitrogen atmosphere (500 mL/min) in the same tube furnace. Activated biochar was washed with 0.002% hydrochloric acid (HCl) until a neutral pH was achieved and dried at 90°C overnight. This final product was designated SCGKOH.

3.2.2 Nitrogen Surface Functionalization

The SCGKOH biochar was modified with nitrogen-containing surface functional groups through two primary methods to facilitate subsequent polymer coating via radical initiated polymerization. In the first method adapted from Yang et al.,[68] nitro (NO_2) groups were introduced to the biochar via electrophilic aromatic substitution and then reduced to amine (NH_2) groups via reduction. First, SCGKOH was mixed with equal volumes of nitric and sulfuric acid at a 1:17 mass:volume ratio (i.e., for every 1 g of SCGKOH, 17 mL of each acid was added). This mixture was placed in an ice bath inside a fume hood and stirred for 3 h to produce SCGKOH-NO2(3h). At the end of the reaction time, the reaction solution was diluted five times with water and filtered using a vacuum pump filter and Whatman GF 100 filter paper (Whatman, United Kingdom) to separate out the biochar product. This biochar was added to 50 mL of ultrapure water (MilliQ; 18.2 MΩ-cm; Millipore Sigma) in a polypropylene tube and rotated at 40 rpm for 30 minutes to wash off residual acid. The wash process was repeated with isopropyl alcohol and the final product was dried at 90°C overnight and stored in an airtight container prior to further modification or

characterization. To reduce nitro groups to amine groups, 2.2 g of SCGKOH-NO2(3h) was added to 22 mL of water along with 8.8 mL of ammonium hydroxide and stirred for 15 min. Then 12.1 g of sodium dithionite was added, and the mixture was stirred for 20 h at 200 rpm. Next, 52.8 mL of acetic acid was added, and the mixture was heated at 98°C under reflux for 5 hours. After the reaction completed, the solution was filtered with Whatman GF 100 filter paper and washed to remove residual reaction solution. Washing steps were as follows: ultrapure water for 1 h, isopropyl alcohol for 1 h, ultrapure water for 30 min. All washes were conducted with 50 mL of wash solution in a polypropylene tube and rotated at 40 rpm. The final product was designated SCGKOH-NH2(3h).

In the second amine modification method adapted from Kasera et al.,[102] a nitrogen source (melamine or ammonium chloride) was added to SCGKOH in water and the mixture was heated to catalyze attachment of nitrogen containing functional groups. Briefly, either melamine or ammonium chloride was measured such that 1 g N was added per 1 g of SCGKOH (e.g., for 1 g of SCGKOH either 0.84 g melamine or 3.98 g ammonium chloride was weighed). The melamine or ammonium chloride was mixed well with ultrapure water (15 mL water per g SCGKOH) and then added with the SCGKOH to a ceramic crucible (VWR, Radnor, PA). The crucible was placed with the lid on in a muffle furnace (Seattle Pottery Supply, Inc., Seattle, WA) at 400°C in an air atmosphere for 1 h and then removed and allowed to cool to room temperature. The final material was rinsed with ultrapure water to remove unreacted chemical and dried at 90°C for 24 h. Modified biochar were designated SCGKOH-M1 (melamine) and SCGKOH-A1 (ammonium chloride). Alternate methods for attaching melamine to SCGKOH were explored and discarded due to lower rates of attachment.

3.2.3 Physicochemical Characterization of Nitrogen Functionalized Biochar

Several types of nitrogen-containing functional groups are commonly found in highly aromatic carbon materials (like biochar) and were expected here based on results of previous studies, including: pyrrolic-N, pyridinic-N, amine-N, graphitic-N, and pyridinic-N^+ oxides.[68,102-104] The structures of these functional groups are detailed in **Figure 3.1**. Pyrrolic, amine, and some types of quaternary nitrogen groups all contain an N–H bond making them able to participate in radical initiated polymerization and were thus the desired types of nitrogen groups for this study. [100,101] The nitrogen functionalized biochar materials produced in section 2.2 were characterized using several techniques discussed below to confirm modification success, characterize the types of nitrogen-containing functional groups, and quantify the coverage and extent of each type.

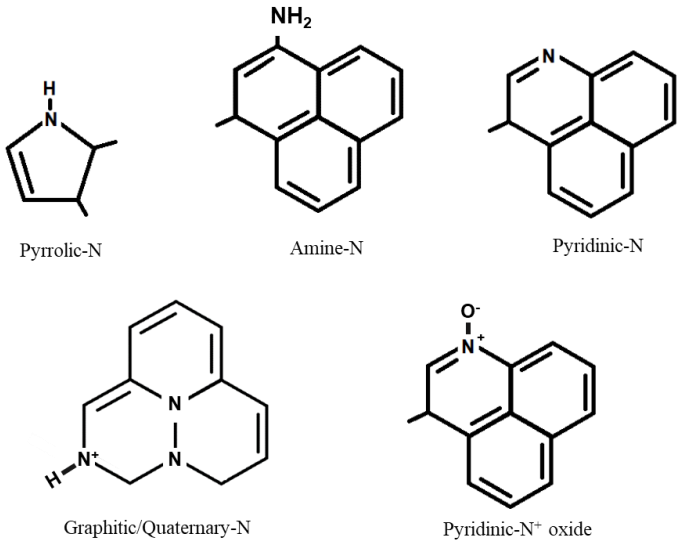

Figure 3.1 Structures of expected nitrogen-containing surface functional groups.

Carbon, hydrogen, nitrogen (CHN) elemental analysis was performed on a Perkin Elmer (Waltham, MA) 2400 Series elemental analyzer to quantify the mass percentages of nitrogen added to the biochar materials during modification.

Two spectroscopic analyses were performed to identify and quantify the types of nitrogen surface functional groups. X-ray photoelectron spectroscopy (XPS) was conducted on a Kratos (Manchester, UK) Axis Ultra DLD X-ray Photoelectron Spectrometer. XPS data was referenced

to a hydrocarbon peak with binding energy of 285.0 eV. Diffuse Reflectance Fourier Transform Infrared Spectroscopy (DRIFTS) measurements were collected on a Thermo Scientific™ (Waltham, MA) Nicolet™ iSTM10 FT-IR Spectrometer using a KBr to biochar mass ratio of 10:1. Collected spectra were corrected with the atmospheric suppression and auto background corrections available in the OMNIC processing software from Thermo Fisher.

3.2.4 Molecularly Imprinted Polymer Coating of Biochar

A layer of molecularly imprinted polymer (MIP) was coated on the surface of the nitrogen-modified biochar materials via thermally activated radical initiated polymerization to increase selectivity of the adsorbent for PFAS compounds. PFOS was chosen as a template compound because: (1) it is known to participate in relatively strong electrostatic and hydrophobic interactions compared to other PFAS increasing the likelihood of successful imprinting in the final polymer;[19,73] (2) it has a relatively long molecule length which should result in MIP binding sites capable of adsorbing a number of equal-length and shorter PFAS;[105,106] and, (3) it is one of the most widely detected PFOS in the environment.[44] Two functional monomers were chosen, one containing a quaternary nitrogen moiety ((vinylbenzyl) trimethylammonium chloride, VBTAC and one containing a fluorocarbon moiety (2-(trifluoromethyl)acrylic acid, TFMA) and were used individually or in combination as described in **Table 3.1**. Quaternary nitrogen moieties have been shown to retain a positive charge over a wide pH range and were expected to electrostatically attract the negatively charged headgroups of most PFAS compounds across environmentally-relevant pH ranges, an important feature for selective PFAS adsorption.[89,91,107,108] The quaternary nitrogen-containing compound was chosen for its similar molecular length to PFOS, a property which has been shown to increase interactions in aqueous systems.[105,106] Fluorocarbon-containing functional monomers have been shown previously to improve adsorption of long chain PFAS

compounds.[91] N,N'-methylenebisacrylamide (MBA) was used as a crosslinker because it has been shown to perform well in aqueous systems[91,100] and 2,2-azobisisobutyronitrile (AIBN) was used as the initiator.

MIP production was accomplished in three steps: pre-polymerization mixing, thermally activated radical initiated polymerization, and template washing. Briefly, approximately 0.213 mmol of PFOS and 0.859 mmol of each functional monomer were added to 167 mL of ultrapure water and stirred at 150 rpm at room temperature for 10 h to allow the template and functional monomers to align. At the same time, 0.5 g of biochar was added to approximately 40 mL of ultrapure water and allowed to sit for 10 h to pre-wet the biochar. At the end of the pre-polymerization time, 8.59 mmol MBA along with the pre-wet biochar was added to the polymerization mixture and mixed for 30 min. Next, 1.00 mmol AIBN was added to initiate polymerization and the reaction solution was mixed at 150 rpm and 60°C for 15 h. Following polymerization, the coated biochar was separated from solution and rinsed with methanol to remove unattached polymer. Finally, the coated biochar was placed in 100 mL of 70% methanol/1% sodium chloride and shaken at 200 rpm and 33°C for 24 h to wash out the template. This process was repeated until the PFOS concentration in the wash solution dropped below 2000 μg/L at which point the biochar was washed for 24 h in ultrapure water and then dried at 60°C overnight. The final product was labeled according to the combination of substrate and functional monomer used as described in **Table 3.1** and stored in a sealed container for further use.

Table 3.1 MIP naming convention by nitrogen modification method and functional monomer selection.

Name	Biochar substrate	VBTAC 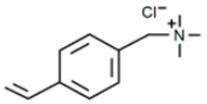	TFMA 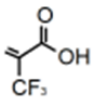
MIP-NV	SCGKOH-NH_2(3h)	Y	-
MIP-AVF	SCGKOH-A1	Y	Y
MIP-MVF	SCGKOH-M1	Y	Y
MIP-MV	SCGKOH-M1	Y	-

VBTAC: (vinylbenzyl) trimethylammonium chloride; TFMA: (2-(trifluoromethyl)acrylic acid

3.2.5 Characterization of Molecularly Imprinted Polymer Layer

Several characterization methods were undertaken to evaluate the success, extent, and thickness of the polymer coating. A JOEL JSM- 6010PLUS/LA Analytical Scanning Electron Microscope (SEM; JOEL, Peabody, MA) was used to image the samples and evaluate any changes in topography or texture. An FEI Tecnai G2 F20 Twin or Tecnai G2 F20 SuperTwin Transmission Electron Microscope (TEM; FEI, Hillsboro, OR) was used to visualize the thickness of the polymer layer and provide insight into the extent of the coating. Specific surface area was measured with nitrogen adsorption at 77K and Brunner-Emmet-Teller (BET) fitting on a Micromeritics 3Flex Analyzer (Micromeritics, Norcross, GA) to quantify changes in surface area resulting from the nitrogen modification and polymer coating processes.

3.2.6 Adsorption Batch Testing

Three adsorption batch tests ranging from simple to complex matrices were performed to evaluate PFAS removal capabilities and selectivity of the MIP coated biochar materials. For all batch tests, 50 mL of water and 5 mg of adsorbent were added to a 50 mL polypropylene tube

along with sufficient volume of methanol-based PFAS (or organic contaminant) stock solution to achieve the desired initial concentration while maintaining a methanol concentration of not more than 0.2%. Samples were prepared in triplicate, rotated for 4 days to achieve equilibrium adsorption state, and filtered and prepared for analysis via LC-MS/MS as discussed in **Appendix A**, **section A7**. First, adsorption of 4471 ± 357 μg/L PFOS was evaluated for all MIP materials in a water only matrix to provide information on the equilibrium adsorption of the template compound by the various MIP materials. Second, adsorption of 1543 ± 217 μg/L PFOS, 1318 ± 173 μg/L perfluorobutanesulfonate (PFBS), and 1453 ± 582 μg/L PFOA combined in an ultrapure water only matrix was evaluated to obtain information on adsorption capabilities for PFAS of different chain length (PFBS) and head group (PFOA) from the template. Sample pH was not adjusted or controlled during these two batch tests, however final pH was measured and found to be approximately 6.5 ± 0.5. Results from these tests were used to screen the MIP-biochar, and MIP-NV, MIP-MVF, and MIP-MV were chosen for further evaluation. Finally, PFAS adsorption was evaluated in a more complex matrix containing compounds representative of key components found in WWTP effluent including representative divalent cations (i.e., 12 mg/L Mg^{2+} as $MgCl_2$ and 26 mg/L Ca^{2+} as $CaCl_2$),[37] sEfOM (i.e., 2.5 mg/L bovine serum albumin, 2 mg/L sodium alginate, 0.5 mg/L octanoic acid, and 5 mg/L humic acid chosen to represent the protein, carbohydrate, fat, and humic components of EfOM, respectively),[37,64-67] PFAS (i.e., 1735 ± 104 μg/L PFOS, 1582 ± 12 μg/L PFOA, and 2313 ± 71 μg/L PFBS), and co-occurring organic contaminants (i.e., 1916 ± 76 μg/L caffeine, 1520 ± 63 μg/L fipronil, and 3385 ± 217 μg/L pentachlorophenol). The pH was adjusted at the start of the test to 7.0 ± 0.1 with sodium hydroxide (NaOH) and buffered with 5 mM HEPES to maintain a constant pH throughout the test. Concentrations of PFAS and co-occurring organics were chosen to be much higher than would be

expected in typical WWTP effluent[30,31,109-111] to better elucidate differences in performance between MIP materials, however total concentrations of PFAS and co-occurring organics were set approximately equal to better represent competition between these species that would be expected in real WWTP systems. EfOM stock solution concentrations were evaluated via total organic carbon analysis using a Sievers 900 Portable TOC analyzer (GE Instruments, Boulder, CO).

3.2.7 Regeneration of Spent Adsorbent

Single cycle regeneration of spent adsorbent was performed following adsorption of PFOS only in the first batch test and following PFAS adsorption in the more complex matrix to better understand how these materials would be expected to perform over multiple use cycles. The regeneration wash solution was chosen to have the same composition as the template washing solution from **section 3.2.5**. Briefly, after collection of LC-MS/MS samples for each adsorption test, the remainder of the adsorption solution was removed and 50 mL of 70% MeOH/1% NaCl was added to each tube of spent adsorbent. Samples were capped, wrapped in parafilm to minimize evaporation of MeOH, and rotated at 40 rpm for 24 h to facilitated desorption. Final concentrations of PFAS were quantified as discussed in **section A7**. a significant portion of the nitrogen from the melamine modified materials is expected not to be active for MIP polymer attachment because it is not bonded to one or more hydrogen atoms (i.e., pyrrolic-N, amine-N, or quaternary-N, see explanation in section 2.3). Percent mass change in oxygen composition, obtained through EA and proximate carbon analysis (PCA), was not directly correlated with percent change in nitrogen composition

3.3 RESULTS AND DISCUSSION

3.3.1 Nitrogen Biochar Modification Approaches Result in Comparable Total Nitrogen Quantities

Results from destructive characterization methods to evaluate material composition reveal an increase in both nitrogen and oxygen composition for all nitrogen modified materials. Elemental analysis (EA) revealed a wide range of nitrogen compositions from 13.0% for SCGKOH-M1 to 1.8% for SCGKOH-NH2(Xh) (**Table 3.2**). It is important to note that a significant portion of the nitrogen from the melamine modified materials is expected not to be active for MIP polymer attachment because it is not bonded to one or more hydrogen atoms (i.e., pyrrolic-N, amine-N, or quaternary-N, see explanation in section 2.3).

Table 3.2 Composition of unmodified and nitrogen modified biochar materials by XPS and elemental analysis.

		SCGKOH	**SCGKOH-NH_2(3h)**	**SCGKOH-M1**	**SCGKOH-A1**
Survey Scan					
Atomic percentage	C	87.1	86.1	81.2	88.5
	O	11.7	10.9	5.3	8.0
	Cl	0.3	0.0	0.0	0.0
	N	0.9	1.8	13.5	3.5
High Resolution					
%N as:	Pyridinic-N	27.6	54.8	61.8	37.0
	Pyrrolic-N	66.2	23.6	24.5	35.9
	Quaternary-N	0.0	10.9	13.7	20.2
	Pyridinic oxide	6.2	10.8	0.0	6.8
Summary					
Total %N from elemental analysis		2.2	1.8	13.0	3.0
Total %NHx-N		0.6	0.8	3.3	1.2

Surface characterization (XPS and DRIFTS) results confirmed that a large percent of the nitrogen functional groups on the SCGKOH-M1 material were theoretically not accessible for polymerization because they did not have an N-H bond; however, the number of sites available for MIP attachment were still noticeably higher for this material than for either the SCGKOH-A1 or SCGKOH-NH_2(3h). Four main types of nitrogen containing surface functional groups were identified via XPS (**Table 3.2**, **Figure 3.2**): pyridinic-N (398.9 ± 0.1eV), pyrrolic-N (400.4 ± 0.2eV), quaternary-N (401.5 ± 0.3eV), and pyridinic-N^+ oxides (403.4 ± 0.8eV).[102-104] Interestingly, amine-N (generally having a binding energy of around 399.5eV) was not identified

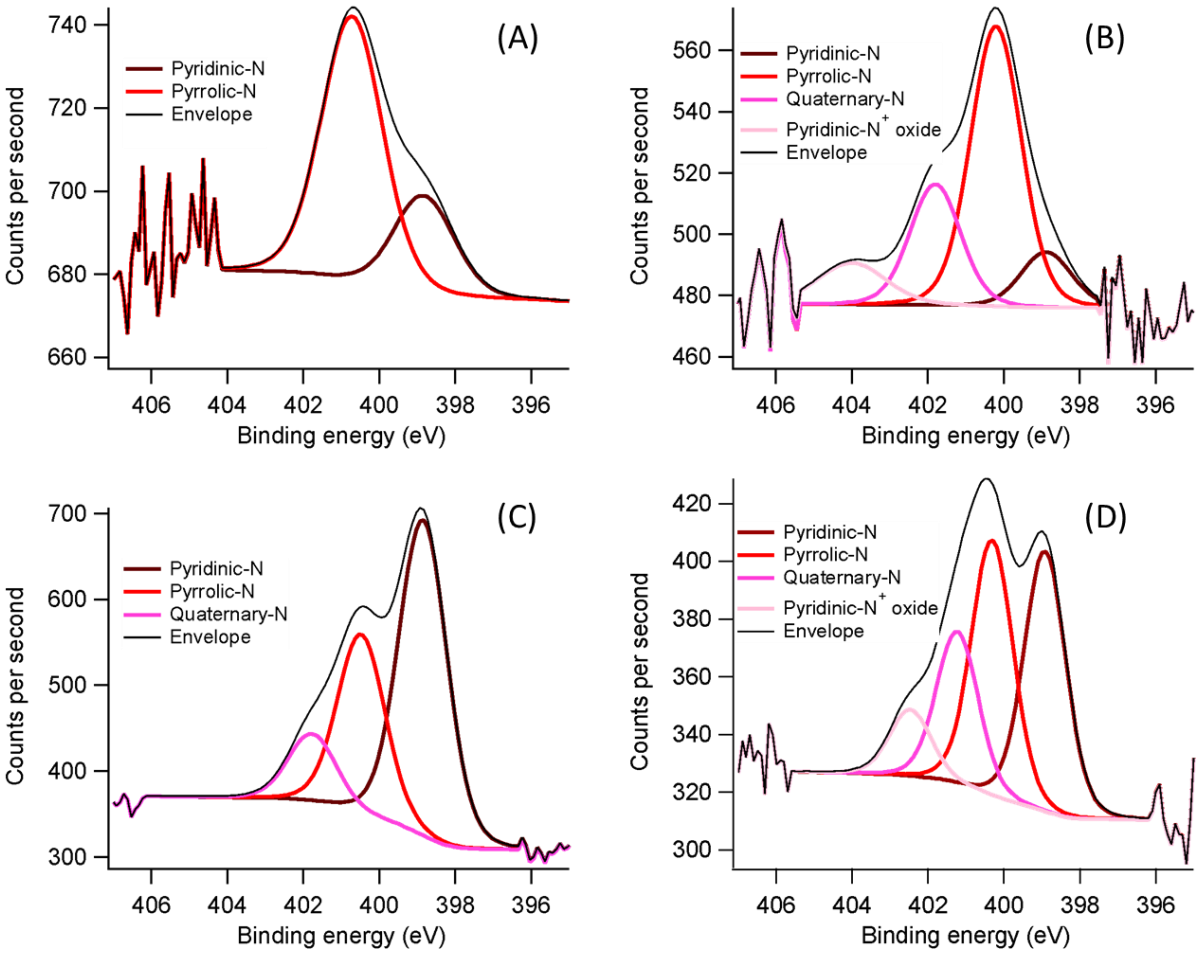

Figure 3.2 Nitrogen (N1s) XPS data for SCGKOH (A), SCGKOH-NH2(3h) (B), SCGKOH-M1 (C), and SCGKOH-A1 (D).

on any of the materials.[102] The unmodified SCGKOH had a low overall density of nitrogen on the surface (0.9 atomic percent) as expected which existed mainly as pyrrolic-N (66.2%) with pyridinic-N comprising a secondary source (27.6%). The ammonium chloride modified biochar (SCGKOH-A1) had a more intermediate nitrogen density (3.5 atomic percent) with similar contributions from pyridinic-N (37.0%), pyrrolic-N (35.9%), and quaternary-N (20.2%). By contrast, the SCGKOH-NH_2(3h) and melamine modified biochar (SCGKOH-M1) contained predominantly pyridinic-N (54.8% and 61.8%) with a secondary contribution from pyrrolic-N (23.6% and 24.5%) and smaller contributions from quaternary-N (10.9% and 13.7%) and pyridinic-N^+ oxide (10.8% and 0.0%). Despite their similar composition, the SCGKOH-M1 had a much higher atomic percentage of nitrogen (13.5%) than the SCGKOH-NH_2(3h) (1.8%). The SCGKOH-M1 also had the highest density of -NH_x groups expected to be available for MIP

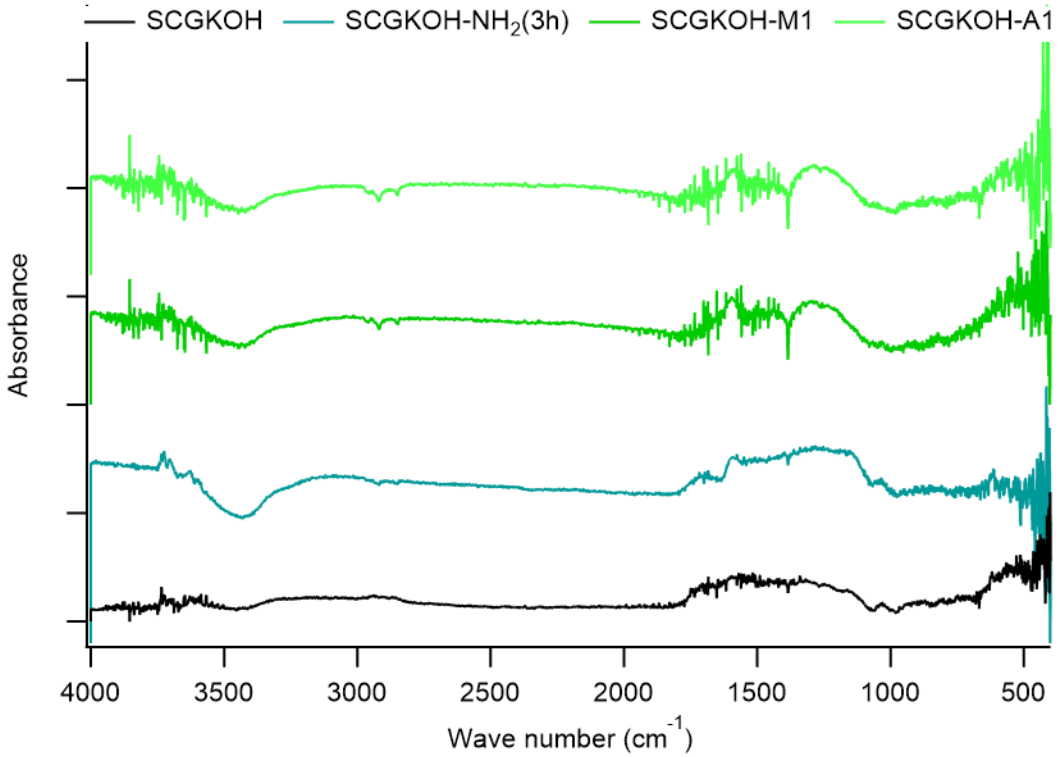

Figure 3.3 DRIFTS spectra of nitrogen modified and unmodified spent coffee grounds biochar.

attachment having approximately 3.3% (atomic percentage) compared to 0.8% and 1.2% for the SCGKOH-NH_2(3h) and SCGKOH-A1, respectively. DRIFTS spectra (**Figure 3.3**) of the SCGKOH-M1 and SCGKOH-A1 show clear peaks at 1600 cm^{-1} and 1250 cm^{-1} that are not present in the spectra from the SCGKOH base material, corresponding to N–H bending and C–N stretching from aromatic amines, respectively.[112] The SCGKOH-NH_2(3h) displayed similar peaks in the same locations although they were harder to distinguish due to their smaller size and the masking effect of the broad band from around 1100 – 1700 cm^{-1} seen on all four biochar materials corresponding to several aromatic and aliphatic hydrocarbon peaks common to activated carbons and biochar.[113] This smaller nitrogen peak size in the SCGKOH-NH_2(3h) spectra agrees well with the finding from XPS analysis that this material has a lower nitrogen density. These results suggest the SCGKOH-M1 substrate may exhibit a faster and more uniform MIP attachment while the other two substrates are expected to experience similar and slightly poorer MIP attachment.

3.3.2 Thicker MIP Coating Significantly Decreases MIP-SCGKOH Composite Specific Surface Area

Successful and relatively uniform MIP coating of the biochar material was verified with TEM (**Figure 3.4**). Imaging revealed MIP coating ranging from 10s to 100s of nm thick across much of the surface for all four materials of interest. Notably, the MIP-MV coating (on the SCGKOH-M1 substrate) was significantly thicker than the other three MIP, with a MIP layer of approximately 200 nm across much of the material surface. SEM imaging was also performed in an effort to further characterize the MIP layer however, the MIP coating was not able to be detected in the resultant images – likely a result of the thin depth of the MIP coating and highly irregular biochar surface making changes in surface structure due to coating hard to distinguish (**Figure 3.4** insets).

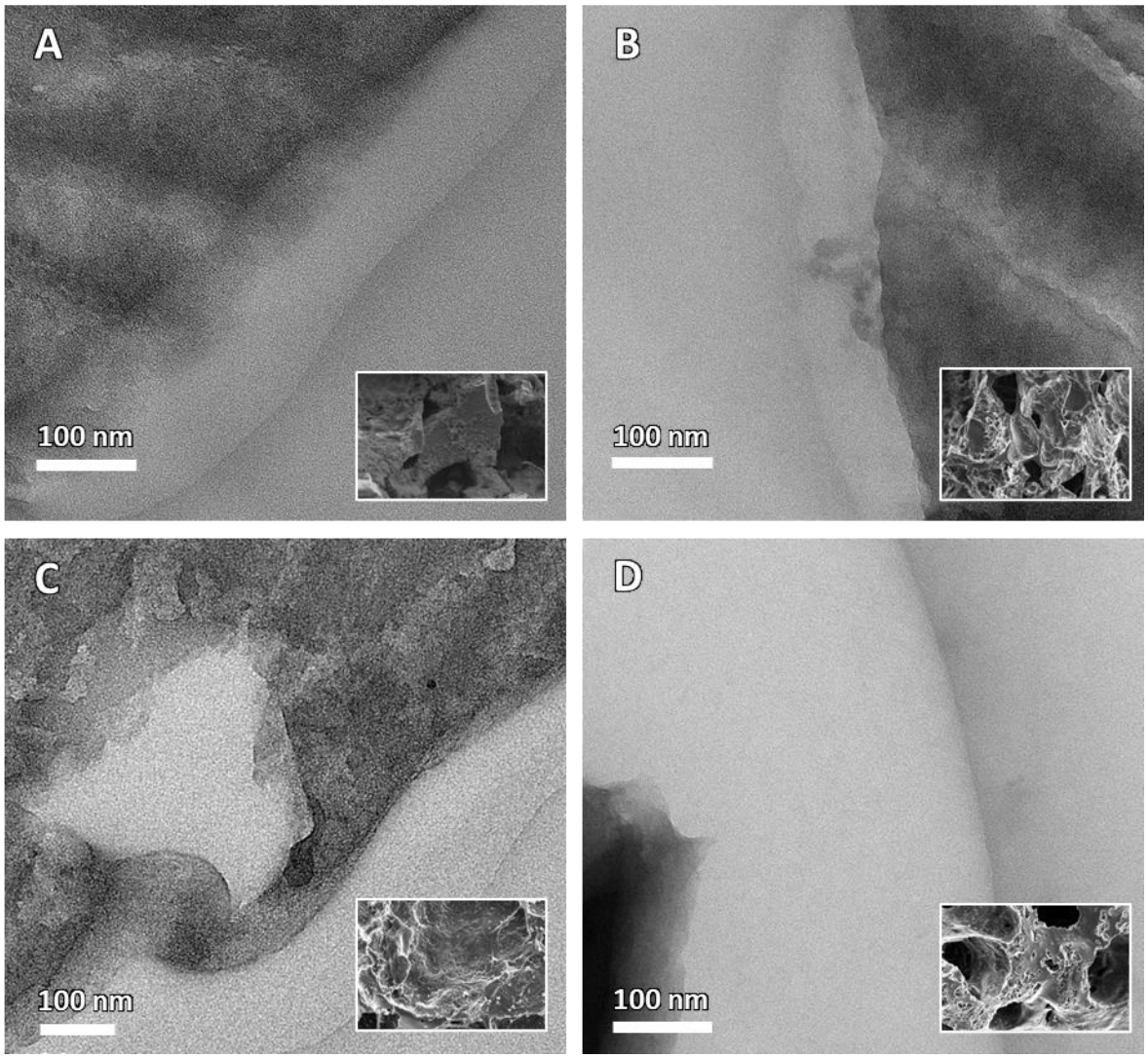

Figure 3.4 TEM images with SEM image insets of MIP modified biochar materials: MIP-NV (A), MIP-AVF (B), MIP-MVF (C), and MIP-MV (D).

MIP coating generally reduced specific surface area (SSA) of the biochar materials, although significant variability in the final SSA was observed based on nitrogen modification method and functional monomer selection. The SSA of MIP-NV and MIP-MVF decreased only slightly from 858 m^2/g for SCGKOH to 741 m^2/g and 806 m^2/g, respectively (**Table 3.3**). By contrast, MIP-MV experienced a significant decrease in SSA to 155 m^2/g which was accompanied by a corresponding increase in average pore size from 1.42 nm for SCGKOH to 8.88 nm. Both observations indicate the MIP coating is likely covering up the smaller micropores in the biochar substrate. Interestingly,

the SSA of the MIP-AVF material increased significantly to 1035 m^2/g, possibly due to increase in SSA of the biochar substrate during nitrogen modification with ammonium chloride. BET analysis of the SCGKOH-A1 was not performed to confirm this finding due to the relatively lower PFAS removal observed for MIP-AVF (discussed in the following sections). BET surface area data indicates the higher nitrogen percentage of the SCGKOH-M1 material results in a more extensive MIP layer which covers up some of the micropores present in the un-coated material, reducing the surface area of the final product for the VBTAC only MIP. This may indicate that more attachment points for the MIP coating is not necessarily beneficial unless other factors like polymerization time or monomer concentration are adjusted. Interestingly, this reduction in BET surface area was not noted when the TFMA monomer was included in the MIP coating. Further work is needed to better understand this relationship.

Table 3.3 Specific surface area of MIP coated and unmodified biochar materials.

Sample Name[1]	**BET SA (m^2/g)**	**Pore Size[2] (nm)**
SCGKOH	858	1.42
MIP-NV	741	1.53
MIP-MVF	806	1.56
MIP-MV	155	8.88
MIP-AVF	1054	1.47
F300[2]	801	2.21

(1) All samples analyzed were #30 – 50 mesh particle size; (2) BJH average pore radius (2V/A).

3.3.3 Adsorption Batch Testing

3.3.3.1 Functional Monomer Choice is a Primary Driver for PFOS Adsorption

PFOS batch test results indicate the VBTAC only and VBTAC + TFMA MIP materials have a distinct PFOS affinity regardless of the modified biochar substrate, as evidenced by comparison of the adsorption data on a surface area normalized basis (**Figure 3.5**). The MIP-MV

and MIP-NV demonstrated similar or slightly greater PFOS removal compared to the unmodified SCGKOH, with adsorption capacities of 0.057, 0.051, and 0.054 mg/m^2, respectively. With the

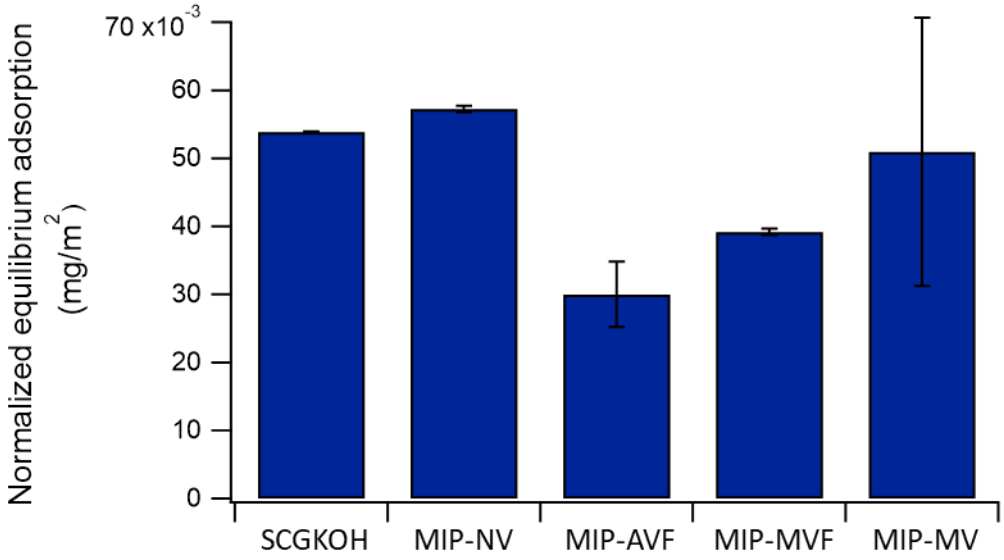

Figure 3.5 Equilibrium adsorption of 4471 ± 371 µg/L PFOS by 100 mg/L MIP modified and unmodified biochar materials in an ultrapure water only matrix following a 4-day equilibration period.

addition of TFMA, the MIP-AVF and MIP-MVF materials demonstrated lower PFOS removal with adsorption capacities of 0.030 and 0.039 mg/m^2, respectively. This finding indicates functional monomer selection has the most significant impact on performance, and any direct impact on PFOS adsorption by surface functional groups resulting from the nitrogen modification processes are similar across all modification methods. The exception to this assumption is the ammonium chloride modification method, which may be negatively impacting PFOS adsorption compared to the other two nitrogen modification methods. This is likely a result of the higher oxygen content of the SCGKOH-A1 (8.0%) compared to the SCGKOH-M1 (5.3%) which is expected to be present in negatively charged surface functional groups that will repel negatively charged PFAS compounds like PFOS.

3.3.3.2 PFAS Competition and MIP Selectivity Resulted in Adsorption of PFOS > PFBS > PFOA

Competition between PFAS compounds combined with the MIP material selectivity for the PFOS template compound resulted in a hierarchy of adsorption affinity observed for all adsorbents: PFOS > PFOA > PFBS (**Figure 3.6**). Adsorption of PFOA was similar to that of PFOS for the SCGKOH and MIP-NV materials with equilibrium adsorption of 0.017 mg PFOS/m^2 and 0.015 mg PFBS/m^2, and 0.019 mg PFOS/m^2 and 0.016 mg PFOA/m^2, respectively. These results confirm the hypothesis that the PFOS template would create a binding site with high affinity for both perfluoroalkyl sulfonic acids (PFSA) and perfluoroalkyl carboxylic acids (PFCA) for the MIP-NV material. For the other three MIPs, however, results indicate higher PFOS selectivity. For example, the PFOA adsorption was approximately half that for PFOS, with adsorption capacities of 0.013 mg PFOS/m^2 and 0.004 mg PFOA/m^2, 0.016 mg PFOS/m^2 and 0.008 mg PFOA/m^2, and 0.033 mg PFOS/m^2 and 0.008 mg PFOA/m^2, for the MIP-AVF, MIP-MVF, and MIP-MV, respectively. The MIP-MV in particular experienced much higher adsorption of PFOS, which is possibly a result of the thicker MIP layer coating observed previously reducing non-specific binding on exposed biochar surfaces. By contrast, adsorption of PFBS was significantly lower than that of PFOS and PFOA for all three materials, which is likely a result of competition between PFAS for easily accessible binding sites. Adsorption capacities of PFBS were 0.009 mg PFBS/m^2, 0.013 mg PFBS/m^2, 0.001 mg PFBS/m^2, 0.004 mg PFBS/m^2, 0.004 mg PFBS/m^2, for the SCGKOH, MIP-NV, MIP-AVF, MIP-MVF, and MIP-MV, respectively. The preferential adsorption of PFOS is not surprising as high selectivity for the template compound is characteristic for MIP materials, however, it is important to note the recovery of PFOA and PFBS is not insignificant. The recovery of a more varied selection of PFAS compounds could potentially be improved through the use of multiple template compounds with varying chain length and charged moieties.

Generally, the total mass of PFAS adsorbed during the competition test decreased slightly from what was observed from the PFOS only test. For example, the MIP-NV material had a normalized PFOS equilibrium adsorption of 0.057 mg/m^2 which decreased to 0.048 mg/m^2 for the PFAS competition test. Similarly, the MIP-MVF material had a normalized PFOS equilibrium adsorption of 0.039 and 0.028 mg/m^2, respectively. The MIP-AVF material in particular experienced a significant decrease in normalized PFOS adsorption (from 0.030 to 0.017 mg/m^2). Therefore, no additional tests were performed using this particular MIP composite material. This finding of decreased PFOS equilibrium adsorption in the presence of other PFAS is likely due to a combination of competition between PFAS compounds and the lower initial concentration of each individual PFAS (1543 ± 217 µg/L PFOS, 1318 ± 173 µg/L PFBS, and 1453 ± 582 µg/L PFOA) compared to the PFOS only test (4471 ± 357 µg/L PFOS). The exception to this general

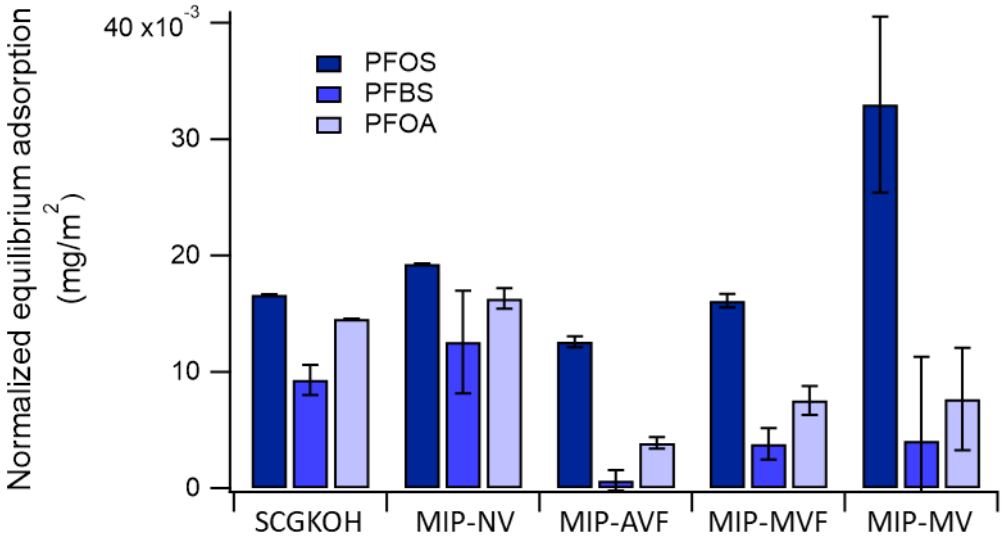

Figure 3.6 Equilibrium adsorption of 1543 ± 217 µg/L PFOS, 1318 ± 173 µg/L PFBS, and 1453 ± 582 µg/L PFOA by 100 mg/L MIP modified and unmodified biochar materials in a water only matrix following a 4-day equilibration period.

observation was the MIP-MV material which demonstrated a comparable mass adsorbed between

the two tests (0.051 and 0.045 mg/m^2). This may indicate the MIP-MV material is less selective for the PFOS template, having a more similar affinity for all three PFAS compounds evaluated.

Interestingly, the TFMA monomer did not appear to improve PFAS adsorption here, contrary findings presented in prior work.[89,91] This was particularly surprising for the more hydrophobic PFAS (i.e., PFOA and PFOS) which have been shown to have a strong affinity for fluorocarbon-containing structures.[89,114,115] More work is needed to determine the exact reason for this finding.

3.3.3.3 Increased Complexity in Reaction Matrix Decreases PFBS Adsorption by MIP Materials

In the more complex matrix containing sEfOM, divalent cations, PFAS, and competing organics, the MIP-NV and MIP-MV adsorbents demonstrated much higher affinity for all three PFAS (i.e., PFOS, PFBS, and PFOA) than the unmodified SCGKOH substrate, while the MIP-MVF demonstrated lower adsorption of all three PFAS. However, the hierarchy of PFAS adsorption remained the same (**Figure 3.7**). PFOS removal remained highest with equilibrium adsorption of 0.011 mg/m^2, 0.022 mg/m^2, 0.007 mg/m^2, and 0.027 mg/m^2 for the SCGKOH, MIP-NV, MIP-MVF, and MIP-MV, respectively. The PFOA removed was again slightly lower for all three MIP coated materials with equilibrium adsorption of 0.013 mg/m^2, 0.006 mg/m^2, 0.017 mg/m^2 for the MIP-NV, MIP-MVF, and MIP-MV, respectively. It is interesting to note the difference in recovery between PFOS and PFOA was less pronounced for the complex matrix test than for the PFAS competition test in the ultrapure water matrix, indicating slightly reduced selectivity for the template compound when salts and competing species are present. The PFBS removal was again lowest with recovered quantities of 0.003 mg/m^2, 0.004 mg/m^2, 0.003 mg/m^2, and 0.013 mg/m^2 for the SCGKOH, MIP-NV, MIP-MVF, and MIP-MV materials, respectively. Notably, the PFBS adsorption on the MIP-MV material is more than three times the mass adsorbed on each of the other materials.

Interestingly, the MIP-MV material displayed an increase in total PFAS adsorbed in the complex matrix (0.140 mg PFAS/m^2) compared to the ultrapure water matrix (0.098 mg PFAS/m^2 or 0.102 mg PFOS/m^2). One possible explanation for this is that swelling of the MIP coating was reduced in the complex matrix due to the higher salt concentration, making more of the binding sites within the inner pores accessible. The effect was likely expressed to a greater extent in the MIP-MV material compared to the other adsorbents because of the greater thickness of the MIP coating. These results are promising for the use of our MIP composite materials in water treatment applications where salts are likely to be present and may improve adsorption capabilities.

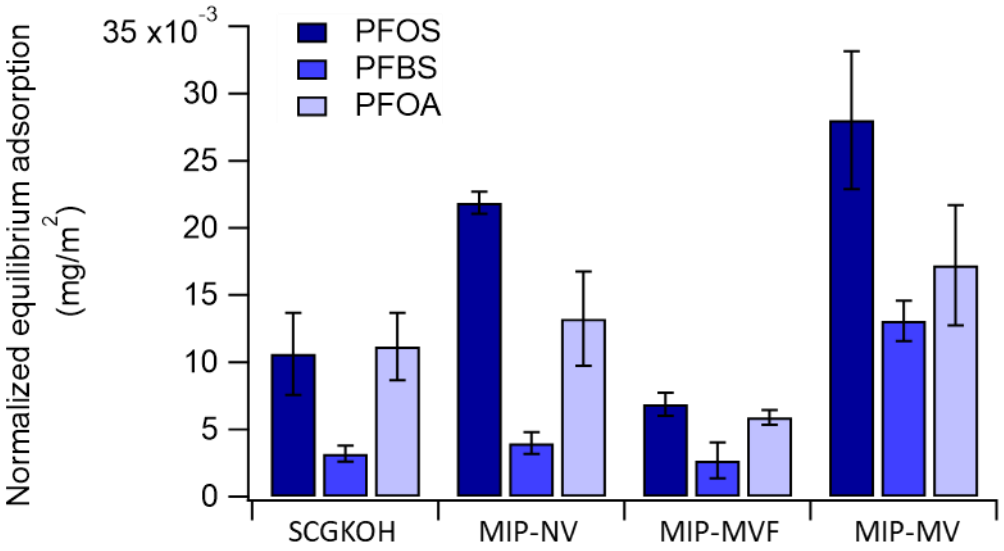

Figure 3.7 Equilibrium adsorption of 1735 ± 104 µg/L PFOS, 1582 ± 12 µg/L PFBS, and 2313 ± 71 µg/L PFOA by 100 mg/L MIP modified and unmodified biochar materials in a complex matrix containing sEfOM (2.5 mg/L bovine serum albumin, 2 mg/L sodium alginate, 0.5 mg/L octanoic acid, and 5 mg/L humic acid), divalent cations (12 mg/L Mg^{2+} as $MgCl_2$ and 26 mg/L Ca^{2+} as $CaCl_2$), and co-occurring organics (1916 ± 76 µg/L caffeine, 1520 ± 63 µg/L fipronil, and 3385 ± 217 µg/L pentachlorophenol) following a 4-day equilibration period.

3.3.4 Regeneration of Spent Adsorbent Indicates Good Potential for Material Reuse

Results from a single cycle regeneration of spent adsorbents indicates high potential for successful material reuse which would increase the functional lifetime of the adsorbent and reduce

capital costs for water treatment. Following PFOS adsorption in the pure water system, nearly complete regeneration of spent adsorbent was observed for both MIP coated and unmodified SCGKOH materials with percent regeneration ranging from 97.5% for MIP-MV to 118.2% for MIP-NV (**Figure 3.8a**). Percent regeneration was calculated as the percent recovery of mass adsorbed during the 4-day equilibrium adsorption test. Adsorbent regeneration following PFAS adsorption in the more complex matrix was more varied and generally followed a similar trend to that observed for adsorption with recovery of PFOS > PFOA > PFBS (**Figure 3.8b**). PFOS recovery decreased slightly to 78.0%, 67.9%, and 69.5% for SCGKOH, MIP-MVF, and MIP-MV, respectively, while PFOS recovery from MIP-NV remained high at 102.1%. PFOA recovery ranged from 71.4% for MIP-NV to 18.8% for MIP-MV, and PFBS recover ranged from 34.9% for MIP-MVF to 19.1% for MIP-MV. The low recovery of PFOA and PFBS from MIP-MV in particular is potentially a result of the thicker MIP coating which may have hindered PFAS desorption kinetics. A comparable material with a thinner MIP coating (e.g., produced using a shorter polymerization time) would likely experience improved regeneration capabilities more similar to that seen for the MIP-NV. Adsorption and regeneration over multiple cycles is needed to obtain a better understanding of the full material lifetime capabilities; however, these preliminary results indicate promising reuse potential in water treatment applications.

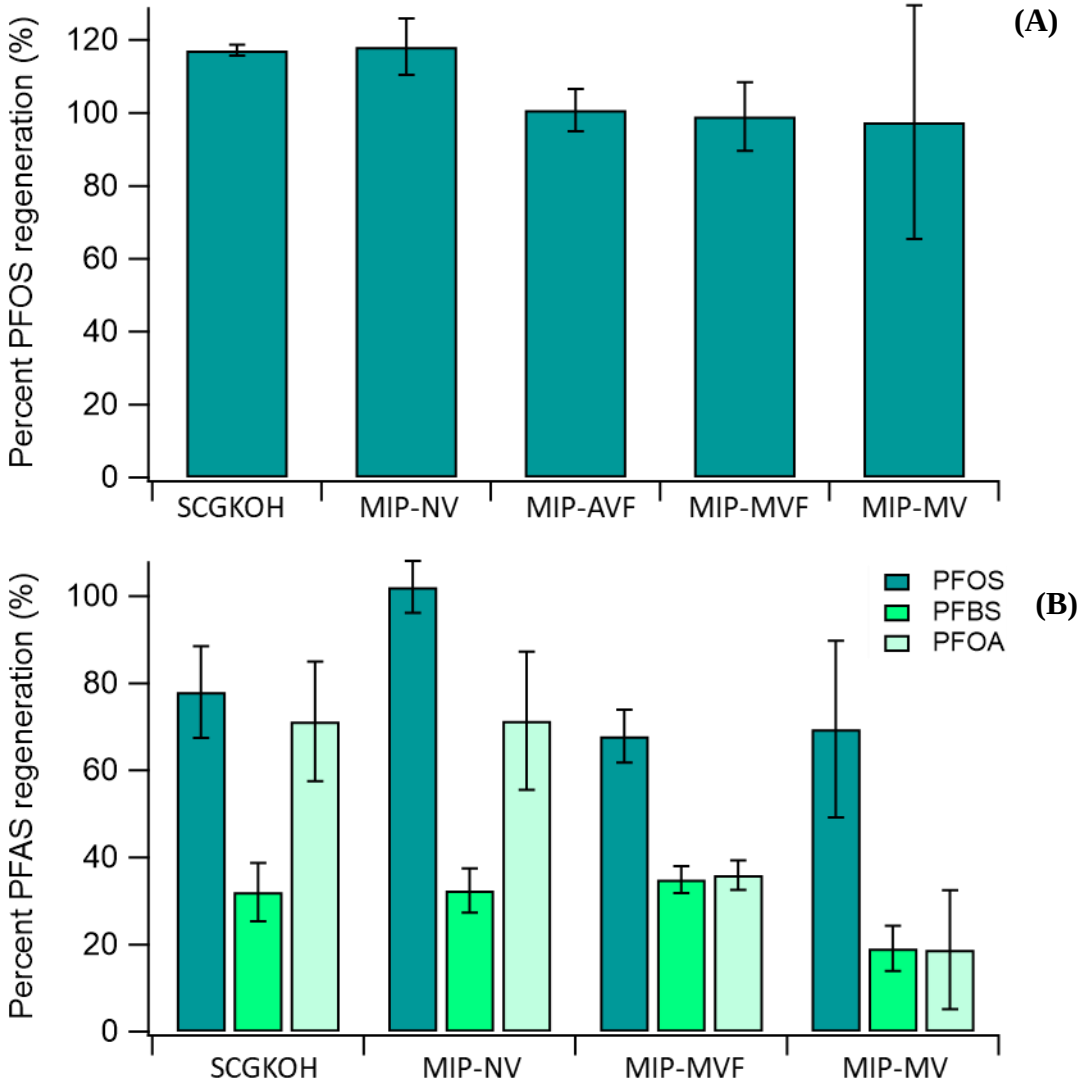

Figure 3.8 Percent recovery of adsorbate from spent adsorbent following batch adsorption tests with (A) of 4471 ± 357 µg/L PFOS only in a water matrix, and (B) 1735 ± 104 µg/L PFOS, 1582 ± 12 µg/L PFBS, and 2313 ± 71 µg/L PFOA adsorption in the complex matrix.

3.4 CONCLUSIONS

Novel nitrogen modification and MIP coating of a spent coffee grounds biochar was successfully performed resulting in an adsorbent material with high potential for PFAS removal in water and wastewater treatment applications. Melamine modification of spent coffee grounds biochar results in the highest fixation of nitrogen containing surface functional groups of the methods explored. All three modification methods increased the oxygen content on the surface of

the biochar with SCGKOH-A1 experiencing the greatest increase, which may have had a slight negative impact on the PFAS removal capabilities of the material. Higher density of nitrogen containing surface functional groups resulted in a thicker MIP layer which decreased the specific surface area and increased the average pore size. Interestingly, the fluorocarbon containing TFMA monomer appeared to decrease the PFAS removal capabilities of the MIP layer. This finding is contrary to findings from previous studies reporting enhanced affinity for PFAS using a fluorinated functional monomer. A hierarchy of PFAS removal and recovery capabilities was observed for all modified and unmodified biochar materials with mass adsorbed/desorbed of PFOS > PFOA > PFBS. Total mass of PFAS adsorbed decreased slightly in the complex matrix containing sEfOM, competing organics, and divalent cations for all materials except the MIP-MV which experienced a slight increase. It is hypothesized that the higher salt concentration in the complex matrix test reduced swelling of the thicker MIP layer for the MIP-MV which would have resulted in a higher surface area and higher PFAS removal capabilities. The nitrogen modification and MIP coating method detailed here is expected to be easily adaptable for any amorphous carbon substrate to produce a highly selective PFAS adsorbate with the potential for multiple regeneration and reuse cycles.

In future work, a shorter polymerization time for the MIP-MV material should be investigated to evaluate the potential for a higher surface area material of the same composition. Further investigation of the impacts of the TFMA monomer on MIP structure and performance could also help elucidate the impacts of the fluorocarbon moiety on PFAS adsorption. Additionally, a multi-template MIP could improve adsorption of shorter chain PFAS compounds by reducing competition between short and long chain PFAS since the long chain PFAS would not be able to access binding sites created by the short chain template. Finally, evaluation of adsorption

performance for PFAS concentrations more representative of those commonly found in WWTP effluent and environmental systems would provide a better understanding of the effectiveness of these adsorbents for water treatment applications.

Chapter 4: Implications and Conclusion

Innovative treatment technologies are needed for the removal of emerging contaminants in water and wastewater treatment to reduce human and environmental exposures to these potentially harmful compounds. One such class of EC that has received significant recent attention are PFAS – a surfactant-like chemical widely used in the manufacture of a range of products. The novel spent coffee grounds biochar described in this research presents an exciting alternative to commercially available activated carbon materials for removal of PFAS in water treatment applications. The widely available food waste feedstock source and relatively low chemical and energy in put requirements for production make this material viable even for low-resource communities. This adsorbent is expected to be particularly effective for removal of PFAS compounds in systems where organic components are low (e.g., drinking water treatment) and has been shown to perform comparably to a commercially available activated carbon, Calgon F300.

Wastewater effluent is increasingly being recognized as an important non-point source of PFAS to environmental systems and, in some cases, to drinking water sources. The spent coffee grounds biochar coated with a PFOS molecularly imprinted polymer described herein are intended to present a prototype for a more cost-effective option for PFAS removal in water treatment applications. The increased selectivity of the material for PFAS compounds compared to non-MIP coated biochar in complex matrices will reduce the need for pretreatment of PFAS-containing waters. Preliminary results for material regeneration show promise for long material lifetimes with multiple reuse cycles possible. The nitrogen modification and polymer coating methods detailed in this study are expected to be easily adapted to any highly aromatic carbon substrate and a range of PFAS templates for synthesis of highly selective adsorbent materials able to be tailored to a variety of treatment needs. Ideally, this technology could be paired with a destructive PFAS

treatment method capable of mineralizing PFAS in the concentrated regeneration solution or otherwise breaking the PFAS down into less toxic end products.

Appendix A: Supplemental Information for Chapter 2

A1. Chemicals and Materials

Calgon Carbon™ Filtrasorb® 300 (F300) was obtained from the Calgon Carbon Corporation (Pittsburg, PA). Mountain Crest Gardens (MCG) biochar was obtained from Cal Forest Nurseries, a subsidiary of GrowPro Inc. located in Etna, CA. MCG is a waste byproduct of mixed softwood (high Ponderosa pine content) combustion energy generation at 1400 °C in a downdraft gasifier. Spent coffee grounds (SCG) were obtained from the University of Washington Bay Laurel Catering Services (Seattle, WA) from their industrial drip coffee makers which use Starbucks® Pike Place® grounds, a medium roast, arabica coffee sourced from Latin America.

All chemicals used were certified ACS reagent grade or equivalent unless otherwise noted. High purity nitrogen gas (99.998%) purchased from Praxair (Danbury, CT) was used for char material production. SCG biochar was activated with sodium hydroxide pellets (NaOH, food grade NF/EP/BP/FCC certification) or potassium hydroxide pellets (KOH) both purchased from Fisher Scientific (Waltham, MA). Activated SCG biochar was washed with hydrochloric acid (HCl, 36.5-38%) purchased from Macron Fine Chemicals™ (VWR International, Radnor, PA). FTIR grade potassium bromide (KBr) for diffuse reflectance infrared Fourier transform spectroscopy (DRIFTS) was obtained from Alfa Aesar (Haverhill, MA), and sodium chloride (NaCl) and nitric acid (HNO_3, 69%) for electrophoretic mobility (EPM) analysis were obtained from VWR Chemical. Samples prepared for EPM analysis were filtered with 0.45 µm, 25 mm diameter nylon syringe filters obtained from VWR. Stock solutions for adsorption experiments were prepared with perfluorooctanesulfonic acid potassium salt (98% purity) purchased from Sigma Aldrich (St. Louis, MO) in Optima™ LC/MS grade Methanol purchased from Thermo Fisher Scientific.

Powdered 4-(2-hydroxyethyl)piperazine-1-ethanesulfonic acid (HEPES, 99.5% purity by titration) purchased from Sigma Aldrich was used to buffer the batch adsorption test solutions and the pH was adjusted with 0.05 M NaOH (food grade NF/EP/BP/FCC certification). Divalent cation stock solution was prepared with calcium chloride ($CaCl_2$) purchased from Sigma Aldrich and magnesium chloride hexahydrate ($MgCl_2$) purchased from VWR Chemical. The simulated wastewater treatment plant effluent organic matter (EfOM) was prepared with bovine serum albumin lyophilized powder (96% purity), alginic acid sodium salt from brown algae (sodium alginate, low viscosity), technical grade humic acid, and octanoic acid (98% purity), all purchased from Sigma Aldrich. Adsorption samples were filtered with 0.2 µm, 25 mm diameter cellulose acetate (CA) syringe filters purchased from Sigma Aldrich or 0.2 µm, 25 mm diameter glass fiber (GF) syringe filters obtained from Foxx Life Sciences (Salem, NH). Analytical and internal PFAS standards were obtained from Wellington Laboratories (Ontario, CA). Reagent Plus® grade powdered caffeine and Pestanal® grade Diuron-d_6 purchased from Sigma Aldrich were used as the analytical and internal standards for caffeine quantification in SCGKOH.

A2. Char Elemental Composition

Proximate carbon analysis was completed using the method detailed in ASTM D1762-84 (reapproved 2007)[59,60]. Briefly, triplicate samples of 0.3 g of char media were weighed and placed in ceramic crucibles. Samples were dried overnight at 100 °C with the crucible lids off and allowed to cool for at least one hour before weighing again to obtain the dry sample weight. Next, samples were heated at 900 °C for six minutes in a muffle furnace to remove the volatile matter. After 6 h, the SCG biochar samples in the ceramic crucible were allowed to cool for one hour before re-weighing. Finally, the SCG biochar samples were heated at 750 °C for 6 h to remove the fixed carbon, and then allowed to cool for at least one hour before collecting a final weight.

Elemental analysis was conducted via a two-step method. First, carbon, hydrogen, and nitrogen percentages were obtained with a Perkin Elmer (Waltham, MA) 2400 Series elemental analyzer. Second, oxygen percentage was calculated as the remainder out of 100% after contributions from carbon, hydrogen, nitrogen, and inorganic components (ash from proximate carbon analysis) were accounted for. Both proximate carbon and elemental analyses were performed using the 297 – 595 µm size fraction of the adsorbent material.

A3. Char Physicochemical Characterization

Caffeine release from SCGKOH was measured via three sequential 24-h equilibration steps followed by liquid chromatography tandem mass spectrometry (LC-MS/MS) quantification of caffeine content in the equilibrium solution. Leaching tests were conducted using the approach described by Belay et al.[116] Preliminary evaluations of caffeine concentrations in water and dichloromethane (as outlined by the Belay et al. colorimetric method) indicated negligible matrix effects in caffeine quantification. Thus, ultrapure water (Milli-Q systems, 18.2 MΩ-cm; Millipore Sigma, Burlington, MA) was used for all further analyses. Briefly, 10 mg of SCG char material (297 – 595 µm size fraction) and 5 mL of ultrapure water were combined in a 15 mL polypropylene tube and rotated at 40 rpm for 24 h. After 24 h, samples were allowed to settle for a few minutes. The supernatant was then decanted, filtered with a 0.2 µm nylon syringe filter, and placed in the refrigerator until analysis. An additional 5 mL of ultrapure water was added to the char material and the process was repeated to obtain caffeine release from a second and third wash.

Table A1. Caffeine content determined by LC-MS/MS, the 1, 2, and 3 designations correspond to the first, second and third washes.

sample ID	caffeine concentration (mg/L)
SCGKOH-1	0.00
SCGKOH-2	0.00
SCGKOH-3	0.00

LC-MS/MS analysis was done with a Waters Corporation (Milford, MA) Quatro Micro quadrupole tandem mass spectrometer preceded by a Phenomenex (Torrence, CA) Gemini 3 µm NX-C18 110A liquid chromatography column as detailed in **section A7**. Results are shown in **Table A1**. The first, second, and third values given represent results from analysis of the first, second, and third equilibrium solutions. Results show no caffeine in the equilibrium wash solutions from SCGKOH indicating low likelihood of caffeine leaching during water treatment applications.

Specific surface area was estimated from nitrogen adsorption data collected at 77 K with a Micromeritics (Norcross, GA) 3Flex instrument using the Brunner-Emmett-Teller (BET) surface area method. Pore size was estimated from the same data using the Barrett, Joyner, and Halenda (BJH) method while pore volume and micropore volume were estimated using the t-method. Approximately 0.1 g of sample was degassed at 300 °C for 12 h prior to data collection. Free space analysis was evaluated with helium gas following nitrogen adsorption. Results are presented in **Table A2**.

Table A2. BET surface area and pore surface area, volume, and diameter for the precursor and activated SCG biochar, F300, and MCG materials.

sample ID[1]	pore SA[2] (m^2/g)		pore size[3] (nm)	
	adsorption	desorption	adsorption	desorption
SCG400 SCG600	No points within BJH pore size interval			
SCG800	0.61	1.25	45.55	22.50
SCGKOH	59.40	52.65	1.42	1.28
MCG	175.05	186.16	2.33	2.17
F300	112.92	121.71	2.21	2.10

1. All samples analyzed were #30 - #50 mesh particle size.
2. BJH cumulative surface area of pores between 0.8500 nm and 150.0000 nm radius
3. BJH average pore radius (2* volume/area)
SA – surface area

Surface zeta potential was measured with a Zetasizer Nano ZS (Malvern Instruments, Malvern, UK). Briefly, 22.9 mg of char material fines (i.e., particles less than 297 µm) were suspended in 22.9 mL of 5 mM NaCl solution and allowed to equilibrate for 24 h. For the MCG biochar surface

zeta potential measurement at pH 7.69, the pH of the solution was then brought to 7.7 ± 0.05 through addition of 1% HNO_3. Prior to analysis the sample was resuspended via sonication for 10 minutes and then filtered with a 0.45 µm nylon filter. Approximately 10 mL of sample volume was wasted through the filter prior to collection of 5 mL of sample for analysis to minimize particle loss across the filter. The solution pH was measured following particle size and zeta potential analysis with a Thermo Scientific (Waltham, MA) Orion™ Star A111 pH meter equipped with an Orion™ PerpHecT™ Ross™ combination pH micro electrode. Results are recorded in **Table A3**.

Table A3. Particle size, poly dispersity index (PDI), zeta potential, and pH measurements for the precursor and activated SCG biochar, F300, and MCG materials.

	particle size (d.nm)	PDI	zeta potential (mV)	pH
SCG400	125.8	0.202	-37.8	7.46
SCG600	127.1	0.216	-47.0	7.45
SCG800	116.4	0.205	-46.2	7.64
SCGKOH	127.0	0.231	-52.0	7.66
F300	193.4	0.455	-21.5	7.68
MCG	372.8	0.377	-26.4	9.29
	232.4	0.339	-26.2	7.69

d.nm = particle diameter in nanometers
PDI = poly dispersity index

Scanning electron microscopy (SEM) imaging of the biochar and activated carbon material morphology was measured with a ThermoFisher Scientific (Waltham, MA) Apreo VP SEM instrument following platinum sputtering of the media where necessary to increase electrical conductivity. Images are shown in **Figure S1**.

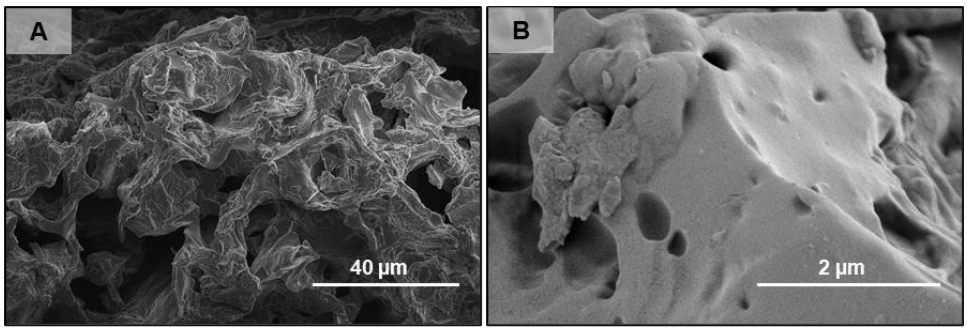

Figure A1. Scanning electron microscopy (SEM) images of the SCG400 precursor at lower (A) and higher (B) magnification.

Fourier transform infrared spectra were collected for the three SCG biochar pyrolysis temperatures, SCGKOH, and MCG with the DRIFTS of the Thermo Scientific™ (Waltham, MA) Nicolet™ iSTM10 FT-IR Spectrometer. DRIFTS spectra were not collected for the F300 material as this information has been well characterized elsewhere [117]. Samples were ground with a mortar and pestle and mixed at a 10:1 mass ratio of KBr to char material (except for MCG which used a 13:1 ratio) to optimize the signal to noise ratio. Results are displayed in **Figure A2** and indicate decreasing peak size and occurrence with increasing pyrolysis temperature and with activation for the SCG char materials. The peaks observed in these spectra are characteristic of highly aromatic carbon materials. In particular, the broad peak observed centered around 1250 cm^{-1} for the SCG400 and SCG600 biochar can be attributed to a C–O stretching vibration [118], the peaks near 1460 cm^{-1} and 1600 cm^{-1} are both attributed to aromatic C=C stretching vibrations [113], the peaks centered around 2900 cm^{-1} (2800 to 3000 cm^{-1}) and the peak at 3050 cm^{-1} are attributed to aromatic C – H stretching vibration [113].

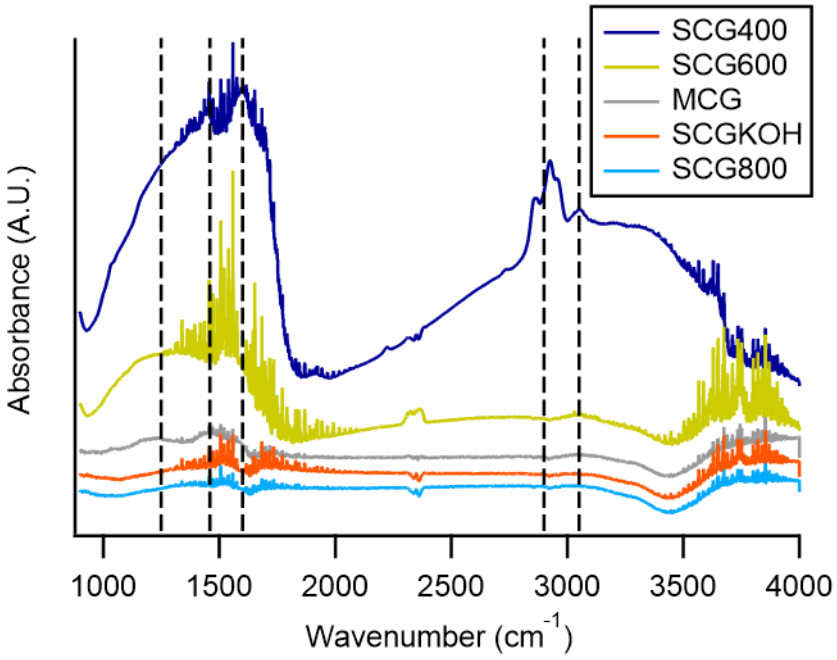

Figure A2. DRIFTS FTIR spectra of activated and precursor SCG biochar, and the MCG biochar. The ratio of KBr to biochar was 10:1 for all SCG char materials and 13:1 for the MCG.

A4. Preliminary Adsorption Tests

Preliminary evaluation of PFOS adsorption was performed with the three pyrolyzed SCG biochar (SCG400, SCG600 and SCG800) to evaluate their PFOS removal capability and to determine to optimal solid:liquid ratios for future adsorption studies. A PFOS stock solution in methanol was used to prepare 50 mL of 46 ± 4 µg/L PFOS in ultrapure water with variable biochar masses to achieve solid:liquid ratios of 50, 100, and 200 mg/L in 50-mL polypropylene centrifuge tubes. Methanol concentrations of no more than 0.2% were maintained in this and subsequent batch tests. This residual methanol is not expected to significantly impact the adsorption processes. Triplicate samples were prepared for each material and rotated at 40 rpm on a Fisherbrand™ (Waltham, MA) multipurpose tube rotator for 24 h. Equilibrated batch test samples were filtered with a 0.20 µm cellulose acetate syringe filter with 20 mL of sample wasted through the filter prior to collection of 5 mL for analysis. Results are displayed in **Figure A3**.

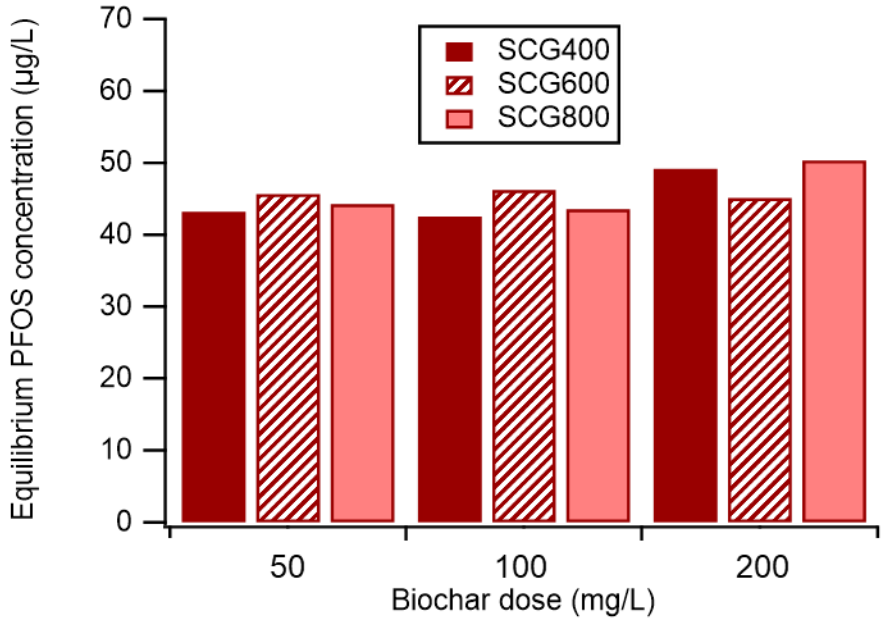

Figure A3. Equilibrium PFOS concentration from an initial concentration 46 ± 4 µg/L PFOS over a 24-h equilibrium batch adsorption test by SCG400, SCG600, and SCG800 at solid (mg biochar) to liquid (L of PFOS solution) ratios of 50, 100, and 200.

A5. PFOS Losses from Sample Filtration

Several filtration options were evaluated for batch adsorption samples to identify a method that would minimize PFOS losses. Two types of filter materials previously shown to result in low PFAS losses were tested: cellulose acetate (CA) and glass fiber (GF) [119]. Both types of filters were 0.2 µm syringe filters, 25 mm in diameter. PFOS loss filtration tests were conducted using 50 mL of ultrapure water in a 50-mL polypropylene tube with initial PFOS concentrations of approximately 5, 50, and 500 µg/L obtained through spiking with concentrated PFOS stock in methanol while maintaining a volumetric methanol concentration in water of no greater than 0.2%. Triplicate samples of each PFOS concentration were rotated at 40 rpm for 5 to 10 minutes after PFOS addition to ensure adequate mixing, and a 500 µL aliquot was then removed to be used as a non-filtered control. Filters were pre-wet with 5 mL of ultrapure water and then approximately 20 mL of sample was wasted through each filter prior to collection of 2 to 3 mL of sample to be used for analysis. The same filter was used for replicates of each concentration, and filters were washed with 20 mL of each new sample before collection of aliquots for analysis. PFOS quantification was done with LC-MS/MS as described in **section A7**.

PFOS loss was calculated as the percent difference between the filtered and non-filtered samples, and results are shown in **Table A4**. Although the GF filter performed well at high concentrations (i.e., negligible PFOS loss across the filter), performance decreased at lower concentrations (14.5% loss at 31.69 µg/L) leading to issues with recovery of sufficient PFOS for sample analysis around 5 µg/L. The CA filter, by contrast, showed more consistent PFOS loss (around 13%) at higher concentrations with decreased loss at low concentrations (1.4% loss at 3.11 µg/L).

Sample purification via centrifugation was also attempted using a method detailed by Zhi and Liu[73] and results were compared to the CA and GF filtration results. Briefly, 5 mg of MCG biochar was added to triplicate samples of 50 mL of ultrapure water in a 50-mL polypropylene tube and spiked with 50 µg/L of PFOS from a concentrated methanol stock. MCG char was chosen for this test because it had significantly more fines observed during sieving and washing than either the F300 or the SCGKOH and thus seemed most likely to exhibit challenges with removal of small particles from solution during centrifugation. A set of control samples without MCG were prepared in the same manner. Samples were rotated at 40 rpm for 24 h to equilibrate and then a 500 µL aliquot was removed from the control samples for a non-centrifuged control. Samples were then centrifuged for 10 minutes at 2300 rpm to remove the large biochar particulates and a 1000 µL aliquot was removed from the center of the supernatant (to avoid floating char particles) and added to a 15-mL polypropylene tube. The aliquot was then diluted with 900 µL of methanol and centrifuged at 4000 rpm for 10 minutes. The supernatant was then divided into a 950 µL volume placed in an LC-MS vial for future analysis and a 950 µL volume placed in a capped and parafilm-sealed test tube in the refrigerator for SEM imaging to evaluate the char removal capabilities of this method. Briefly, a 1 × 0.5 inch silicon wafer was washed with ethanol and allowed to dry in a dust free area. A 5 µL drop of each MCG sample was placed on the mirrored side of the wafer and allowed to dry in a dust free area for SEM analysis.

Results from the PFOS analysis of the centrifuged and non-centrifuged ultrapure water sample showed negligible PFOS loss from centrifugation (**Table A4**). However, SEM imaging indicated the presence of a significant amount of both fine MCG particulates and those greater than 0.2 µm in diameter, making this a non-viable option for char removal from PFOS adsorption testing with char material adsorbents. Therefore, the CA filtration method, including pre-wetting of the filter

material and wasting of 20 mL of sample prior to collection of an aliquot for analysis, was selected and used for the kinetics, isotherm, and effluent organic matter and divalent cation effects tests.

Table A4. PFOS losses during sample purification via centrifugation and filtration with glass fiber or cellulose acetate membranes.

purification method	concentration (ppb)	% loss
glass fiber	31.69	14.2%
	422.09	-0.5%
cellulose acetate	4.11	1.4%
	31.79	13.9%
	369.77	12.0%
Centrifugation	37.64	-3.7%

A6. Simulated Effluent Organic Matter, Divalent Cation Solution, and HEPES Buffer

Stock solutions of BSA, sodium alginate, and humic acid were prepared by mixing 20 mg of powdered compound in 20 mL of ultrapure water, covering with parafilm, and mixing for 24-hours. Total organic carbon (TOC) concentrations of each stock solution were measured with a Shimadzu (Kyoto, Japan) TOC-L analyzer. The divalent cations, Ca^{2+} and Mg^{2+}, were added at concentrations of 26 mg/L (0.65 mM) and 12 mg/L (0.5 mM), respectively to mimic concentrations typically present in wastewater treatment plant effluent.[120]

The effect of HEPES buffer on PFOS adsorption was evaluated for the SCGKOH in the presence of divalent cations to confirm minimal interference by the buffer. HEPES was chosen as a buffer compound for: (1) its circumneutral pKa (7.0)[63] which is typical of the mid-range pH values associated with wastewater treatment plant effluent (i.e., the focus of this study);[121] (2) its lack of reaction with other species in the batch test aquatic matrices as predicted by Visual MINTEQ;[122] and, (3) its use in similar prior studies as an appropriate buffer for complex aqueous systems containing divalent cations.[61-63] Briefly, 5 mg of SCGKOH was added to 50 mL of ultrapure water in a 50-mL polypropylene tube. An initial PFOS concentration of 91 ± 8 µg/L was achieved by spiking with a concentrated PFOS stock in methanol. Where applicable, HEPES was

added at 5 mM and divalent cations were added at 26 mg/L of Ca^{2+} (0.65 mM) and 12 mg/L of Mg^{2+} (0.5 mM). Triplicate samples were rotated at 40 rpm for 24 h before filtration and LC-MS sample preparation as described previously. Results are shown in **Figure A4** and indicate improved adsorption of PFOS in the presence of divalent cations and minimal effect of the HEPES buffer on PFOS adsorption.

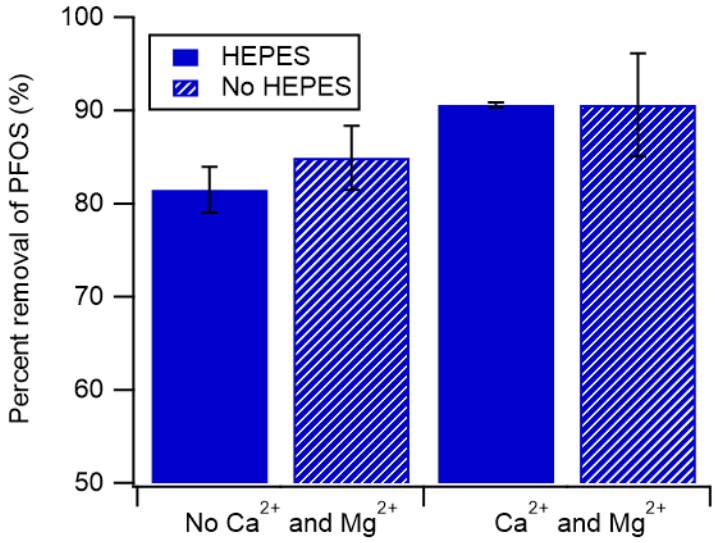

Figure A4. Percent removal of 91 ± 8 µg/L PFOS by 100 mg/L SCGKOH with and without calcium (26 mg/L) and magnesium (12 mg/L) ions in the presence and absence of 5 mM HEPES buffer.

A7. Liquid Chromatography Mass Spectrometry Methodology

PFOS ($C_8F_{17}SO_3$; **Figure A5A)** was analyzed with a Waters (Milford, MA) Quattro Micro API triple quadrupole tandem mass spectrometer (MS/MS) preceded by liquid chromatography (LC) using an Agilent (Santa Clara, CA) Zorbax Rapid Resolution Eclipse XBD-18C column (2.1 x 50 mm, 1.8 µm). An Agilent, XDB-C18 guard cartridge (80Å, 4.6 x 12.5 mm, 5 µm) was placed before the LC column to pre-filter the sample. The MS/MS operation mode was set to negative electrospray ionization with multiple reaction monitoring (MRM) transitions (**Table A5**). The LC was operated with a stationary phase of HPLC grade water with 10 mM ammonium acetate (A) and a mobile phase of HPLC grade methanol with 10 mM ammonium acetate (B). Details of the

gradient program are given in **Table A6**. Mass labeled PFOS (mPFOS) was used as an internal standard. Calibration standards and samples were prepared with 50:50 volumetric ratio of methanol and water to minimize PFOS losses to the tube walls.

Caffeine ($C_8H_{10}N_4O_2$; **Figure A5, B)** was analyzed with a Waters Corporation (Milford, MA) Quattro Micro quadrupole tandem mass spectrometer (MS/MS) preceded by a Phenomenex (Torrence, CA) Gemini 3 μm NX-C18 110A (3 x 50 mm) liquid chromatography column. The MS operation mode was set to positive electrospray ionization with MRM transitions (**Table A5**). The LC was operated with a stationary phase of acetonitrile and methanol at a 50:50 volumetric ratio (A) and a mobile phase of 10 mM ammonium acetate in HPLC grade water (B). Details of the gradient program are given in **Table A7**. Diuron-d6 was used an internal standard. All liquid chemicals used in LC-MS/MS analysis of PFOS and caffeine were Optima® LCMS Grade and the Ammonium Acetate was certified ACS Grade (98.1% purity), all purchased from Fisher Chemical (Hampton, NH).

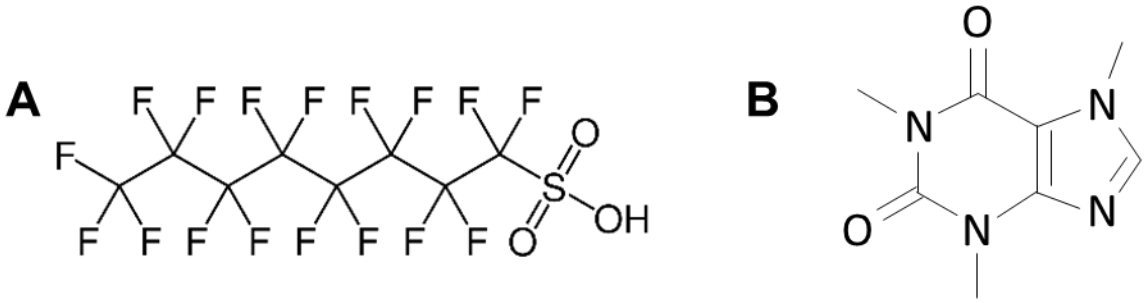

Figure A5. Chemical structures of PFOS (A) and caffeine (B).

Table A5. LC-MS/MS parameters used for quantification of PFOS and caffeine.

	ionization mode	parent (m/z)	product ion (m/z)	cone energy (V)	collision energy (V)	RT (min)
PFOS	-	498.95	79.40	53	40	9.808
PFOS	-	498.95	98.50	53	35	9.840
mPFOS	-	503.10	79.40	53	40	9.800
Caffeine	+	195.15	138.15	32	23	3.17
Caffeine	+	195.15	110.15	32	20	3.17
Diuron-d6	+	239.15	52.05	27	15	5.33
Diuron-d6	+	239.15	52.05	27	18	5.33

Table A6. LC gradient program for elution of PFOS using 10 mM ammonium acetate in water and methanol as the stationary and mobile phases.

time (min)	%A (10 mM ammonium acetate)	%B (10 mM ammonium acetate in methanol)	flow rate (mL/min)
0.0	80	20	0.4
8.0	5	95	0.4
10.0	5	95	0.4
10.5	80	20	0.4
16.0	80	20	0.4

Table A7. LC gradient program for elution of caffeine using acetonitrile and methanol (50:50 v/v ratio) as the stationary phase, and 10 mM ammonium acetate in water as the stationary phase.

time (min)	%A (acetonitrile and methanol 50:50 v/v)	%B (10 mM ammonium acetate)	flow rate (mL/min)
0.0	90	10	0.2
1.5	45	55	0.2
4.0	36	64	0.2
5.0	1	99	0.2
7.0	1	99	0.2
7.5	90	90	0.3
10.0	90	90	0.2

BATCH TEST MODEL CALCULATIONS

A8. Kinetics Model Calculations

Three models were employed to evaluate the kinetic PFOS adsorption data for the SCGKOH, F300, and MCG. The first two were linear fits of the pseudo first order (PFO) and pseudo second order (PSO) kinetic models, commonly used to describe adsorption kinetics for a range of adsorbent materials and contaminants.[19,123,124] Pseudo-alpha-order reactions are those that in actuality depend on the concentrations of multiple reactants but in practice are assumed to depend on the concentration of only one reactant (i.e., PFOS) because the others are present in excess.[125] The equations for these models are as follows:

$$\frac{dq_t}{dt} = k_1(q_e - q_t) \quad \text{Eq. (A.1)}$$

$$\ln(q_e - q_t) = \ln(q_e) - k_1 t \quad \text{Eq. (A.2)}$$

$$\frac{dq_t}{dt} = k_2(q_e - q_t)^2 \quad \text{Eq. (A.3)}$$

$$\frac{t}{q_t} = \frac{1}{k_2 q_e^2} + \frac{t}{q_e} \quad \text{Eq. (A.4)}$$

where q_t and q_e are the PFOS adsorption density at time t and at equilibrium in mg PFOS/g char material; t is time in hours; and k_1 and k_2 are the PFO and PSO kinetic rate constants.

For the linear PFO model, a graph of the natural log of ($q_e - q_t$) was plotted as a function of time, and the equilibrium adsorption capacity (q_e) was evaluated as the adsorption capacity at five days to calculate the y-variables. The rate constant (k_1) and equilibrium adsorption capacity (q_e) were then determined using Eq. (A.2) and the slope and intercept of this graph. For the linear PSO model, a graph of t/q_t versus time was plotted, and the rate constant (k_2) and equilibrium adsorption capacity (q_e) were then solved using Eq. (A.4) and the slope and intercept of this graph.

A modified non-linear PFO model derived from the Langmuir kinetic adsorption model (Eq. A.5) by Liu and Shen was the third model used to fit the PFOS adsorption data for all three char materials.[72] The relevant equations for this model are as follows:

$$\frac{d\theta_t}{dt} = k_a C_t(1-\theta_t) - k_d\theta_t = k_1(\theta_e - \theta_t) + k_2(\theta_e - \theta_t)^2 \quad \text{Eq. (A.5)}$$

$$\frac{k_1}{k_2} = \frac{\sqrt{K_L^2(C_0 - q_{max}X)^2 + 2K_L(C_0 + q_{max}X) + 1}}{K_L q_{max} X} \quad \text{Eq. (A.6)}$$

$$\theta_e = \frac{K_L(q_{max}X + C_0) + 1 - \sqrt{K_L^2(C_0 - q_{max}X)^2 + 2K_L(C_0 + q_{max}X) + 1}}{2K_L q_{max} X} \quad \text{Eq. (A.7)}$$

$$\theta_t = \theta_e\left(1 - e^{-k_1 t}\right) \quad \text{Eq. (A.8)}$$

$$\theta_t = \frac{(C_e - C_t) * M_{ads}}{q_{max}} = \frac{q_t}{q_{max}} \quad \text{Eq. (A.9)}$$

where θ_t and θ_e are the fraction of PFOS adsorption sites occupied at time t and at equilibrium; t is time in hours; k_a, k_d, k_1, and k_2 are the adsorption and desorption, and first and second order kinetic rate constants, respectively; K_L is the Langmuir adsorption constant; q_{max} is the maximum adsorption capacity determined by the Langmuir adsorption isotherm; X is the concentration of adsorbent (g/L); C_0, C_e, and C_t are the PFOS concentration at time zero, equilibrium, and time t, respectively; and M_{ads} is the mass (g) of adsorbent. Liu and Shen determined that if the ratio of k_1/k_2 is greater than or equal to θ_e, the Langmuir kinetic model reduces to the PFO model; if the

ratio of k_1/k_2 is instead much smaller than θ_e, the Langmuir model reduces to the PSO model; and for all other conditions, the full Langmuir kinetic model applies. This relationship was evaluated for the kinetic adsorption data from the SCGKOH, F300, and MCG adsorbents using Eq. (A.6) and Eq. (A.7), and the PFO derivation of the Langmuir kinetic model (Eq. A.8) was found to be accurate for all three materials at PFOS concentrations below 3200, 3100, and 5200 µg/L for SCGKOH, F300, and MCG, respectively. The non-linear PFO derivation of the Langmuir kinetic model was applied for all three char materials using Eq. (A.8). Briefly, the value for θ_e can be solved from the Langmuir adsorption isotherm parameters as shown in Eq. (A.7) while experimental values for θ_t can be solved from experimentally determined PFOS solution concentrations using Eq. (A.9). The rate constant (k_1) was solved using the Microsoft Excel® solver function to minimize the square error between experimental and theoretical values of θ_t. The goodness of fit of the linear PFO and PSO and the non-linear PFO kinetic models were compared using the square error as shown in **Figure A6**.

A9. Adsorption Isotherm Model Calculations

Adsorption isotherm data for the three char materials were fit to both the Langmuir and Freundlich adsorption isotherm models whose original and linear forms are given below as Eq. (A.10) through Eq. (A.13):[75]

$$q_e = \frac{q_{max} K_L C_e}{1 + K_L C_e} \quad \text{Eq. (A.10)}$$

$$\frac{C_e}{q_e} = \frac{1}{q_{max}} C_e + \frac{1}{K_L q_{max}} \quad \text{Eq. (A.11)}$$

$$q_e = K_F C_e^{1/n} \quad \text{Eq. (A.12)}$$

$$\log(q_e) = \frac{1}{n}\log(C_e) + \log(K_F) \quad \text{Eq. (A.13)}$$

where q_e and q_{max} were the equilibrium and maximum adsorption densities, C_e is the equilibrium adsorbate concentration, K_L and K_F are the Langmuir and Freundlich adsorption rate constants, respectively, and *1/n* is the Freundlich coefficient of non-linearity.

For both models, experimental data was transformed to the appropriate linear variables shown in Eq. (A.11) and (A.13) and plotted to obtain linear isotherm values for the model parameters (q_{max} and K_L for the Langmuir model and K_F and $1/n$ for the Freundlich model) from the slope and intercept of the plotted data. Non-linear isotherm values for the model parameters were also obtained through minimization of the square error between experimentally and theoretically derived equilibrium adsorption densities (q_e) using the Microsoft Excel® solver function. Theoretical values for q_e were obtained using Eq. (A.10) and (A.12) with the linearly derived isotherm values as starting points. In all cases the non-linear model parameters provided a better fit for the data and were used for all further analysis and discussion.

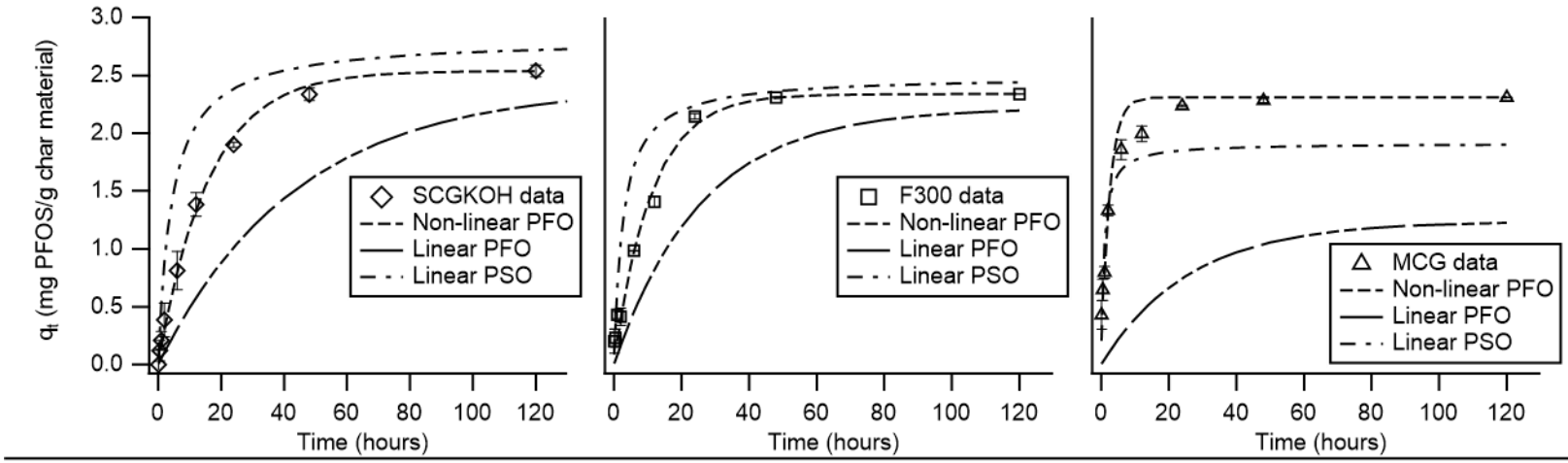

		non-linear pseudo first order		linear pseudo first order			linear pseudo second order			
	$q_{e,exp}$ (mg/g)	k_1 (h^{-1})	σ^2	$q_{e,calc}$ (mg/g)	k_1 (h)	σ^2	$q_{e,calc}$ (mg/g)	v_0 (mg/g*h)	log ($K_{d,eq}$) (L/kg)	σ^2
SCGKOH	2.538	0.069	0.003	2.480	0.065	0.025	2.818	0.230	5.359	0.232
F300	2.337	0.090	0.016	2.343	0.148	0.023	2.495	0.368	6.212	0.183
MCG	2.309	0.414	0.040	2.169	0.483	1.137	2.337	1.680	6.762	0.083

Figure A6. Kinetics modeling of PFOS adsorption rates onto (a) SCGKOH, (b) F300, and (c) MCG with the Langmuir-derived non-linear pseudo first order, linear pseudo first order, and linear pseudo second order models.

REFERENCES

(1) Foley, J. A.; Ramankutty, N.; Brauman, K. A.; Cassidy, E. S.; Gerber, J. S.; Johnston, M.; Mueller, N. D.; O'Connell, C.; Ray, D. K.; West, P. C. Solutions for a cultivated planet. *Nature* **2011**, *478* (7369), 337-342.

(2) Molden, D.; Frenken, K.; Barker, R.; De Fraiture, C.; Mati, B.; Svendsen, M.; Sadoff, C. W.; Finlayson, M.; Atapattu, S.; Giordano, M. *Trends in water and agricultural development*; International Water Management Institute, 2007.

(3) Lu, J.; Vecchi, G. A.; Reichler, T. Expansion of the Hadley cell under global warming. *Geophysical Research Letters* **2007**, *34* (6).

(4) USEPA, U., CDM Smith. 2012 Guidelines for Water Reuse. Office of Wastewater Management, O. o. W., Ed.; U.S. EPA,: Washington, D.C., 2012.

(5) Scruggs, C. E.; Thomson, B. M. Opportunities and challenges for direct potable water reuse in arid inland communities. *Journal of Water Resources Planning and Management* **2017**, *143* (10), 04017064.

(6) Inyang, M.; Dickenson, E. The potential role of biochar in the removal of organic and microbial contaminants from potable and reuse water: a review. *Chemosphere* **2015**, *134*, 232-240. DOI: https://doi.org/10.1016/j.chemosphere.2015.03.072.

(7) Inyang, M.; Dickenson, E. R. V. The use of carbon adsorbents for the removal of perfluoroalkyl acids from potable reuse systems. *Chemosphere* **2017**, *184*, 168-175. DOI: https://doi.org/10.1016/j.chemosphere.2017.05.161.

(8) Bolong, N.; Ismail, A.; Salim, M. R.; Matsuura, T. A review of the effects of emerging contaminants in wastewater and options for their removal. *Desalination* **2009**, *239* (1-3), 229-246.

(9) Barzen-Hanson, K. A.; Roberts, S. C.; Choyke, S.; Oetjen, K.; McAlees, A.; Riddell, N.; McCrindle, R.; Ferguson, P. L.; Higgins, C. P.; Field, J. A. Discovery of 40 classes of per- and polyfluoroalkyl substances in historical aqueous film-forming foams (AFFFs) and AFFF-impacted groundwater. *Environ. Sci. Technol.* **2017**, *51* (4), 2047-2057. DOI: 10.1021/acs.est.6b05843.

(10) Hu, X. C.; Andrews, D. Q.; Lindstrom, A. B.; Bruton, T. A.; Schaider, L. A.; Grandjean, P.; Lohmann, R.; Carignan, C. C.; Blum, A.; Balan, S. A.; et al. Detection of poly- and perfluoroalkyl substances (PFASs) in U.S. drinking water linked to industrial sites, military fire training areas, and wastewater treatment plants. *Environ. Sci. Technol. Lett.* **2016**, *3* (10), 344-350. DOI: 10.1021/acs.estlett.6b00260.

(11) Li, F.; Duan, J.; Tian, S.; Ji, H.; Zhu, Y.; Wei, Z.; Zhao, D. Short-chain per-and polyfluoroalkyl substances in aquatic systems: Occurrence, impacts and treatment. *Chem. Eng. J.* **2020**, *380*, 122506.

(12) Houtz, E. F.; Higgins, C. P.; Field, J. A.; Sedlak, D. L. Persistence of perfluoroalkyl acid precursors in AFFF-impacted groundwater and soil. *Environ. Sci. Technol.* **2013**, *47* (15), 8187-8195. DOI: 10.1021/es4018877.

(13) Fenton, S. E.; Ducatman, A.; Boobis, A.; DeWitt, J. C.; Lau, C.; Ng, C.; Smith, J. S.; Roberts, S. M. Per-and polyfluoroalkyl substance toxicity and human health review: Current state of knowledge and strategies for informing future research. *Environ. Toxicol. Chem.* **2021**, *40* (3), 606-630.

(14) IRIS Toxicological Review of Perfluorobutanoic Acid (PFBA) and Related Compound Ammonium Perfluorobutanoic Acid (Public Comment and External Review Draft, 2021). U.S. Environmental Protection Agency: Washington, DC, 2021.
(15) Tsuda, S. Differential toxicity between perfluorooctane sulfonate (PFOS) and perfluorooctanoic acid (PFOA). *J. Toxicol. Sci.* **2016**, *41* (Special), SP27-SP36. DOI: 10.2131/jts.41.sp27.
(16) Mueller, R.; Yingling, V. History and use of per-and polyfluoroalkyl substances (PFAS). *Interstate Technology & Regulatory Council* **2017**.
(17) Buck, R. C.; Franklin, J.; Berger, U.; Conder, J. M.; Cousins, I. T.; De Voogt, P.; Jensen, A. A.; Kannan, K.; Mabury, S. A.; van Leeuwen, S. P. Perfluoroalkyl and polyfluoroalkyl substances in the environment: terminology, classification, and origins. *Integr. Environ. Assess. Manag.* **2011**, *7* (4), 513-541.
(18) USEPA. Interim Guidance on the Destruction and Disposal of Perfluoroalkyl and Polyfluoroalkyl Substances and Materials Containing Perfluoroalkyl and Polyfluoroalkyl Substances. U.S. Environmental Protection Agency,: Washington D.C., 2020.
(19) Xiao, X.; Ulrich, B. A.; Chen, B.; Higgins, C. P. Sorption of poly- and perfluoroalkyl substances (PFASs) relevant to aqueous film-forming foam (AFFF)-impacted groundwater by biochars and activated carbon. *Environ. Sci. Technol.* **2017**, *51* (11), 6342-6351. DOI: 10.1021/acs.est.7b00970.
(20) Washington State Department of Ecology. Per-and Polyfluoroalkyl Substances Chemical Action Plan. Hazardous Waste and Toxics Reduction Program, Ed.; Washington State Department of Ecology,: Olympia, Washington, 2021.
(21) Moody, C. A.; Field, J. A. Perfluorinated surfactants and the environmental implications of their use in fire-fighting foams. *Environ. Sci. Technol.* **2000**, *34* (18), 3864-3870. DOI: 10.1021/es991359u.
(22) Cadore, A.; Chou, C.-H.; Jones, D. G.; Llados, F.; Pohl, H. R. Draft Toxicological Profile for Perfluoroalkyls. U.S. Agency for Toxic Substances and Disease Registry: Atlanta, GA, 2009.
(23) ATSDR. Toxicological Profile for Perfluoroalkyls. Agency for Toxic Substances and Disease Registry,: 2021.
(24) CDC. *Fourth national report on human exposure to environmental chemicals*; US Department of Health and Human Services,, Centers for Disease Control and Prevention, Atlanta, GA, 2009. https://www.cdc.gov/exposurereport/ (accessed 1/7/2020).
(25) Post, G. B.; Cohn, P. D.; Cooper, K. R. Perfluorooctanoic acid (PFOA), an emerging drinking water contaminant: a critical review of recent literature. *Environmental research* **2012**, *116*, 93-117.
(26) IARC monographs on the evaluation of the carcinogenic risk of chemicals to man. **1972**.
(27) van Raalte, D. H.; Li, M.; Pritchard, P. H.; Wasan, K. M. Peroxisome proliferator-activated receptor (PPAR)-α: a pharmacological target with a promising future. *Pharmaceutical research* **2004**, *21* (9), 1531-1538.
(28) USEPA. Drinking water health advisories for PFOA and PFOS. U.S. Environmental Protection Agency, Ed.; 2016.
(29) Thompson, K. A.; Mortazavian, S.; Gonzalez, D. J.; Bott, C.; Hooper, J.; Schaefer, C. E.; Dickenson, E. R. V. Poly- and Perfluoroalkyl Substances in Municipal Wastewater Treatment Plants in the United States: Seasonal Patterns and Meta-Analysis of Long-Term Trends and Average Concentrations. *ACS ES&T Water* **2022**. DOI: 10.1021/acsestwater.1c00377.
(30) Phong Vo, H. N.; Ngo, H. H.; Guo, W.; Hong Nguyen, T. M.; Li, J.; Liang, H.; Deng, L.; Chen, Z.; Hang Nguyen, T. A. Poly-and perfluoroalkyl substances in water and wastewater: A

comprehensive review from sources to remediation. *J. Water Process. Eng.* **2020**, *36*, 101393. DOI: 10.1016/j.jwpe.2020.101393.
(31) Furl, C. V.; Meredith, C. A.; Strynar, M. J.; Nakayama, S. F. Relative importance of wastewater treatment plants and non-point sources of perfluorinated compounds to Washington State rivers. *Sci. Total Environ.* **2011**, *409* (15), 2902-2907. DOI: https://doi.org/10.1016/j.scitotenv.2011.04.035.
(32) Arvaniti, O. S.; Stasinakis, A. S. Review on the occurrence, fate and removal of perfluorinated compounds during wastewater treatment. *Sci. Total Environ.* **2015**, *524-525*, 81-92. DOI: https://doi.org/10.1016/j.scitotenv.2015.04.023.
(33) Loganathan, B. G.; Sajwan, K. S.; Sinclair, E.; Senthil Kumar, K.; Kannan, K. Perfluoroalkyl sulfonates and perfluorocarboxylates in two wastewater treatment facilities in Kentucky and Georgia. *Water Res.* **2007**, *41* (20), 4611-4620. DOI: https://doi.org/10.1016/j.watres.2007.06.045.
(34) Sinclair, E.; Kannan, K. Mass loading and fate of perfluoroalkyl surfactants in wastewater treatment plants. *Environ. Sci. Technol.* **2006**, *40* (5), 1408-1414. DOI: 10.1021/es051798v.
(35) USEPA. Memorandum Regarding Per- and Polyfluoroalkyl Substances. U.S. Environmental Protection Agency: Washington, D.C., 2021.
(36) Yu, J.; Lv, L.; Lan, P.; Zhang, S.; Pan, B.; Zhang, W. Effect of effluent organic matter on the adsorption of perfluorinated compounds onto activated carbon. *J. Hazard. Mater.* **2012**, *225-226*, 99-106. DOI: https://doi.org/10.1016/j.jhazmat.2012.04.073.
(37) Steigerwald, J. M.; Ray, J. R. Adsorption behavior of perfluorooctanesulfonate (PFOS) onto activated spent coffee grounds biochar in synthetic wastewater effluent. *JHM Letters* **2021**, *2*, 100025. DOI: https://doi.org/10.1016/j.hazl.2021.100025.
(38) USEPA. EPA PFAS action plan: program update. U.S. Environmental Protection Agency, Ed.; Washington D.C., 2020.
(39) USEPA. Human health toxicity values for hexafluoropropylene oxide (HFPO) dimer acid and its ammonium salt (CASRN 13252-13-6 and CASRN 62037-80-3) also known as "GenX chemicals". U.S. Environmental Protection Agency, Ed.; Washington D.C., 2018.
(40) Song, X.; Vestergren, R.; Shi, Y.; Huang, J.; Cai, Y. Emissions, transport, and fate of emerging per- and polyfluoroalkyl substances from one of the major fluoropolymer manufacturing facilities in China. *Environ. Sci. Technol.* **2018**, *52* (17), 9694-9703. DOI: 10.1021/acs.est.7b06657.
(41) DuPont. DuPont GenX processing aid for making fluoropolymer resins: setting a new industrial standard for sustainable replacement technology. www.genx.dupont.com.
(42) McNamara, J. D.; Franco, R.; Mimna, R.; Zappa, L. Comparison of activated carbons for removal of perfluorinated compounds from drinking water. *J. Am. Water Work. Assoc.* **2018**, *110* (1), E2-E14. DOI: 10.5942/jawwa.2018.110.0003.
(43) Becker, A. M.; Gerstmann, S.; Frank, H. Perfluorooctanoic acid and perfluorooctane sulfonate in the sediment of the roter main river, Bayreuth, Germany. *Environ. Pollut.* **2008**, *156* (3), 818-820. DOI: https://doi.org/10.1016/j.envpol.2008.05.024.
(44) Arvaniti, O. S.; Hwang, Y.; Andersen, H. R.; Stasinakis, A. S.; Thomaidis, N. S.; Aloupi, M. Reductive degradation of perfluorinated compounds in water using Mg-aminoclay coated nanoscale zero valent iron. *Chem. Eng. J.* **2015**, *262*, 133-139. DOI: https://doi.org/10.1016/j.cej.2014.09.079.
(45) Plumlee, M. H.; Larabee, J.; Reinhard, M. Perfluorochemicals in water reuse. *Chemosphere* **2008**, *72* (10), 1541-1547. DOI: https://doi.org/10.1016/j.chemosphere.2008.04.057.

(46) Washington Department of Health. *Draft recommended state action levels for per- and polyfluoroalkyl substances (PFAS) in drinking water: approach, methods and supporting information*; Chapter 246-290 WAC; Washington Department of Health, Office of Environmental Public Health Sciences, 2019. https://www.doh.wa.gov/Portals/1/Documents/4200/PFASToxicologicalAssessment.pdf (accessed 5/6/2020).
(47) New York State Department of Health. Drinking water quality council recommends nation's most protective maximum contaminant levels for three unregulated contaminants in drinking water. New York State Department of Health,: Albany, NY, 2018.
(48) New Jersey Department of Health. Per- and Polyfluoroalkyl Substances (PFAS) in Drinking Water. Environmental and occupational health surveillance program, New Jersey Department of Health, Ed.; 2020.
(49) Kearns, J. P.; Wellborn, L. S.; Summers, R. S.; Knappe, D. R. U. 2,4-D adsorption to biochars: effect of preparation conditions on equilibrium adsorption capacity and comparison with commercial activated carbon literature data. *Water Res.* **2014**, *62*, 20-28. DOI: https://doi.org/10.1016/j.watres.2014.05.023.
(50) Linares-Solano, Á.; Lillo-Ródenas, M. A.; Lozar, J. P. M.; Kunowsky, M.; Anaya, A. J. R. NaOH and KOH for preparing activated carbons used in energy and environmental applications. *International Journal of Energy, Environment and Economics* **2012**, *2* (4), 59 - 91.
(51) Deng, S.; Nie, Y.; Du, Z.; Huang, Q.; Meng, P.; Wang, B.; Huang, J.; Yu, G. Enhanced adsorption of perfluorooctane sulfonate and perfluorooctanoate by bamboo-derived granular activated carbon. *J. Hazard. Mater.* **2015**, *282*, 150-157. DOI: https://doi.org/10.1016/j.jhazmat.2014.03.045.
(52) Laksaci, H.; Khelifi, A.; Trari, M.; Addoun, A. Synthesis and characterization of microporous activated carbon from coffee grounds using potassium hydroxides. *J. Clean. Prod.* **2017**, *147*, 254-262. DOI: https://doi.org/10.1016/j.jclepro.2017.01.102.
(53) Alcaraz, L.; Escudero, M. E.; Alguacil, F. J.; Llorente, I.; Urbieta, A.; Fernández, P.; López, F. A. Dysprosium removal from water using active carbons obtained from spent coffee ground. *Nanomaterials-Basel* **2019**, *9* (10). DOI: 10.3390/nano9101372 From NLM.
(54) Nguyen, V.-T.; Nguyen, T.-B.; Chen, C.-W.; Hung, C.-M.; Vo, T.-D.-H.; Chang, J.-H.; Dong, C.-D. Influence of pyrolysis temperature on polycyclic aromatic hydrocarbons production and tetracycline adsorption behavior of biochar derived from spent coffee ground. *Bioresour. Technol.* **2019**, *284*, 197-203. DOI: https://doi.org/10.1016/j.biortech.2019.03.096.
(55) Kim, M.-S.; Min, H.-G.; Koo, N.; Park, J.; Lee, S.-H.; Bak, G.-I.; Kim, J.-G. The effectiveness of spent coffee grounds and its biochar on the amelioration of heavy metals-contaminated water and soil using chemical and biological assessments. *J. Environ. Manage.* **2014**, *146*, 124-130. DOI: https://doi.org/10.1016/j.jenvman.2014.07.001.
(56) Rajapaksha, A. U.; Chen, S. S.; Tsang, D. C. W.; Zhang, M.; Vithanage, M.; Mandal, S.; Gao, B.; Bolan, N. S.; Ok, Y. S. Engineered/designer biochar for contaminant removal/immobilization from soil and water: potential and implication of biochar modification. *Chemosphere* **2016**, *148*, 276-291. DOI: https://doi.org/10.1016/j.chemosphere.2016.01.043.
(57) Ulrich, B. A.; Im, E. A.; Werner, D.; Higgins, C. P. Biochar and activated carbon for enhanced trace organic contaminant retention in stormwater infiltration systems. *Environ. Sci. Technol.* **2015**, *49* (10), 6222-6230. DOI: 10.1021/acs.est.5b00376.

(58) Ray, J. R.; Shabtai, I. A.; Teixidó, M.; Mishael, Y. G.; Sedlak, D. L. Polymer-clay composite geomedia for sorptive removal of trace organic compounds and metals in urban stormwater. *Water Res.* **2019**, *157*, 454-462. DOI: https://doi.org/10.1016/j.watres.2019.03.097.
(59) ASTM International. *ASTM D1762-84, standard test method for chemical analysis of wood charcoal*; ASTM International, West Conshohocken, PA, 2007. www.astm.org (accessed 6/19/2020).
(60) Mukherjee, A.; Zimmerman, A. R.; Harris, W. Surface chemistry variations among a series of laboratory-produced biochars. *Geoderma* **2011**, *163* (3), 247-255. DOI: https://doi.org/10.1016/j.geoderma.2011.04.021.
(61) Lee, S.; Uliana, A.; Taylor, M. K.; Chakarawet, K.; Bandaru, S. R. S.; Gul, S.; Xu, J.; Ackerman, Cheri M.; Chatterjee, R.; Furukawa, H.; et al. Iron detection and remediation with a functionalized porous polymer applied to environmental water samples. *Chemical Science* **2019**, *10* (27), 6651-6660, 10.1039/C9SC01441A. DOI: 10.1039/C9SC01441A.
(62) Hafeznezami, S.; Zimmer-Faust, A. G.; Jun, D.; Rugh, M. B.; Haro, H. L.; Park, A.; Suh, J.; Najm, T.; Reynolds, M. D.; Davis, J. A.; et al. Remediation of groundwater contaminated with arsenic through enhanced natural attenuation: Batch and column studies. *Water Res* **2017**, *122*, 545-556. DOI: 10.1016/j.watres.2017.06.029 From NLM.
(63) Miera, R. E. Investigation of Acetaminophen and Caffeine Removal Using Manganese Oxides and Granular Activated Carbon in Column Experiments. University of New Mexico, Albuquerque, NM, 2018. https://digitalrepository.unm.edu/ce_etds/220.
(64) Motsa, M. M.; Mamba, B. B.; Verliefde, A. R. D. Forward osmosis membrane performance during simulated wastewater reclamation: fouling mechanisms and fouling layer properties. *J. Water Process. Eng.* **2018**, *23*, 109-118. DOI: https://doi.org/10.1016/j.jwpe.2018.03.007.
(65) Miranda-García, N.; Suárez, S.; Sánchez, B.; Coronado, J. M.; Malato, S.; Maldonado, M. I. Photocatalytic degradation of emerging contaminants in municipal wastewater treatment plant effluents using immobilized TiO2 in a solar pilot plant. *Appl. Catal. B.* **2011**, *103* (3), 294-301. DOI: https://doi.org/10.1016/j.apcatb.2011.01.030.
(66) Tang, L.; Li, L.; Chen, R.; Wang, C.; Ma, W.; Ma, X. Adsorption of acetone and isopropanol on organic acid modified activated carbons. *J. Environ. Chem. Eng.* **2016**, *4* (2), 2045-2051. DOI: https://doi.org/10.1016/j.jece.2016.03.031.
(67) Dittmar, S.; Zietzschmann, F.; Mai, M.; Worch, E.; Jekel, M.; Ruhl, A. S. Simulating effluent organic matter competition in micropollutant adsorption onto activated carbon using a surrogate competitor. *Environ. Sci. Technol.* **2018**, *52* (14), 7859-7866. DOI: 10.1021/acs.est.8b01503.
(68) Yang, G.-X.; Jiang, H. Amino modification of biochar for enhanced adsorption of copper ions from synthetic wastewater. *Water Res.* **2014**, *48*, 396-405. DOI: https://doi.org/10.1016/j.watres.2013.09.050.
(69) Gromov, A.; Dittmer, S.; Svensson, J.; Nerushev, O. A.; Perez-García, S. A.; Licea-Jiménez, L.; Rychwalski, R.; Campbell, E. E. B. Covalent amino-functionalisation of single-wall carbon nanotubes. *J. Mater. Chem.* **2005**, *15* (32), 3334-3339, 10.1039/B504282H. DOI: 10.1039/B504282H.
(70) Du, Z.; Deng, S.; Bei, Y.; Huang, Q.; Wang, B.; Huang, J.; Yu, G. Adsorption behavior and mechanism of perfluorinated compounds on various adsorbents—a review. *J. Hazard. Mater.* **2014**, *274*, 443-454. DOI: https://doi.org/10.1016/j.jhazmat.2014.04.038.
(71) Moussout, H.; Ahlafi, H.; Aazza, M.; Maghat, H. Critical of linear and nonlinear equations of pseudo-first order and pseudo-second order kinetic models. *Karbala International Journal of Modern Science* **2018**, *4* (2), 244-254. DOI: https://doi.org/10.1016/j.kijoms.2018.04.001.

(72) Liu, Y.; Shen, L. From langmuir kinetics to first- and second-order rate equations for adsorption. *Langmuir* **2008**, *24* (20), 11625-11630. DOI: 10.1021/la801839b.
(73) Zhi, Y.; Liu, J. Adsorption of perfluoroalkyl acids by carbonaceous adsorbents: effect of carbon surface chemistry. *Environ. Pollut.* **2015**, *202*, 168-176. DOI: https://doi.org/10.1016/j.envpol.2015.03.019.
(74) Simonin, J.-P. On the comparison of pseudo-first order and pseudo-second order rate laws in the modeling of adsorption kinetics. *Chem. Eng. J.* **2016**, *300*, 254-263. DOI: https://doi.org/10.1016/j.cej.2016.04.079.
(75) Crittenden, J. C.; Howe, K. J.; Hand, D. W.; Tchobanoglous, G.; Trussell, R. R. *Principles of water treatment*; Hoboken, New Jersey : John Wiley & Sons, Inc., 2012.
(76) Yu, Q.; Zhang, R.; Deng, S.; Huang, J.; Yu, G. Sorption of perfluorooctane sulfonate and perfluorooctanoate on activated carbons and resin: kinetic and isotherm study. *Water Res.* **2009**, *43* (4), 1150-1158. DOI: https://doi.org/10.1016/j.watres.2008.12.001.
(77) Johnson, R. L.; Anschutz, A. J.; Smolen, J. M.; Simcik, M. F.; Penn, R. L. The adsorption of perfluorooctane sulfonate onto sand, clay, and iron oxide surfaces. *J. Chem. Eng. Data* **2007**, *52* (4), 1165-1170. DOI: 10.1021/je060285g.
(78) Higgins, C. P.; Luthy, R. G. Sorption of perfluorinated surfactants on sediments. *Environ. Sci. Technol.* **2006**, *40* (23), 7251-7256. DOI: 10.1021/es061000n.
(79) Steigerwald, J. M.; Peng, S.; Ray, J. R. Novel Perfluorooctanesulfonate-Imprinted Polymer Immobilized on Spent Coffee Grounds Biochar for Selective Removal of Perfluoroalkyl Acids in Synthetic Wastewater. *ACS ES&T Engineering* **2023**. DOI: 10.1021/acsestengg.2c00336.
(80) PFAS Strategic Roadmap: EPA's commitments to Action 2021 - 2024. U.S. Environmental Protection Agency: Washington D.C., 2021.
(81) Vestergren, R.; Cousins, I. T. Tracking the pathways of human exposure to perfluorocarboxylates. *Environ. Sci. Technol.* **2009**, *43* (15), 5565-5575.
(82) Lang, J. R.; Allred, B. M.; Field, J. A.; Levis, J. W.; Barlaz, M. A. National estimate of per-and polyfluoroalkyl substance (PFAS) release to US municipal landfill leachate. *Environ. Sci. Technol.* **2017**, *51* (4), 2197-2205.
(83) Masoner, J. R.; Kolpin, D. W.; Cozzarelli, I. M.; Smalling, K. L.; Bolyard, S. C.; Field, J. A.; Furlong, E. T.; Gray, J. L.; Lozinski, D.; Reinhart, D. Landfill leachate contributes per-/poly-fluoroalkyl substances (PFAS) and pharmaceuticals to municipal wastewater. *Environ. Sci. Water Res. Technol.* **2020**, *6* (5), 1300-1311.
(84) Chen, W.; Zhang, X.; Mamadiev, M.; Wang, Z. Sorption of perfluorooctane sulfonate and perfluorooctanoate on polyacrylonitrile fiber-derived activated carbon fibers: in comparison with activated carbon. *RSC Adv.* **2017**, *7* (2), 927-938, 10.1039/C6RA25230C. DOI: 10.1039/C6RA25230C.
(85) Okaikue-Woodi, F. E.; Cherukumilli, K.; Ray, J. R. A critical review of contaminant removal by conventional and emerging media for urban stormwater treatment in the United States. *Water Res.* **2020**, *187*, 116434.
(86) Davis, M. L. Chapter 12: General Wastewater Collection and Treatment Decision Considerations. In *Water and Wastewater Engineering: Design Principles and Practice*, McGraw Hill, 2011.
(87) Benotti, M. J.; Trenholm, R. A.; Vanderford, B. J.; Holady, J. C.; Stanford, B. D.; Snyder, S. A. Pharmaceuticals and Endocrine Disrupting Compounds in U.S. Drinking Water. *Environ. Sci. Technol.* **2009**, *43* (3), 597-603. DOI: 10.1021/es801845a.

(88) Horst, J.; McDonough, J.; Ross, I.; Houtz, E. Understanding and Managing the potential by-products of PFAS destruction. *Ground Water Monit. Remediat.* **2020**, *40* (2), 17-27.
(89) Takayose, M.; Nishimoto, K.; Matsui, J. A fluorous synthetic receptor that recognizes perfluorooctanoic acid (PFOA) via fluorous interaction obtained by molecular imprinting. *Analyst* **2012**, *137* (12), 2762-2765, 10.1039/C2AN15936H. DOI: 10.1039/C2AN15936H.
(90) Glasscott, M. W.; Vannoy, K. J.; Kazemi, R.; Verber, M. D.; Dick, J. E. μ-MIP: Molecularly Imprinted Polymer-Modified Microelectrodes for the Ultrasensitive Quantification of GenX (HFPO-DA) in River Water. *Environ. Sci. Technol. Lett.* **2020**, *7* (7), 489-495. DOI: 10.1021/acs.estlett.0c00341.
(91) Guo, H.; Liu, Y.; Ma, W.; Yan, L.; Li, K.; Lin, S. Surface molecular imprinting on carbon microspheres for fast and selective adsorption of perfluorooctane sulfonate. *J. Hazard. Mater.* **2018**, *348*, 29-38. DOI: https://doi.org/10.1016/j.jhazmat.2018.01.018.
(92) Kazemi, R.; Potts, E. I.; Dick, J. E. Quantifying Interferent Effects on Molecularly Imprinted Polymer Sensors for Per- and Polyfluoroalkyl Substances (PFAS). *Anal. Chem.* **2020**, *92* (15), 10597-10605. DOI: 10.1021/acs.analchem.0c01565.
(93) Chi, T.-Y.; Chen, Z.; Kameoka, J. Perfluorooctanesulfonic Acid Detection Using Molecularly Imprinted Polyaniline on a Paper Substrate. *Sensors* **2020**, *20* (24), 7301. DOI: 10.3390/s20247301.
(94) Cao, F.; Wang, L.; Yao, Y.; Wu, F.; Sun, H.; Lu, S. Synthesis and application of a highly selective molecularly imprinted adsorbent based on multi-walled carbon nanotubes for selective removal of perfluorooctanoic acid. *Environ. Sci. Water Res. Technol.* **2018**, *4* (5), 689-700, 10.1039/C7EW00443E. DOI: 10.1039/C7EW00443E.
(95) Gauczinski, J.; Liu, Z.; Zhang, X.; Schönhoff, M. Surface Molecular Imprinting in Layer-by-Layer films on Silica Particles. *Langmuir* **2012**, *28* (9), 4267-4273. DOI: 10.1021/la205027j.
(96) Tran.T, T.; Li, J.; Feng, H.; Cai, J.; Yuan, L.; Wang, N.; Cai, Q. Molecularly imprinted polymer modified TiO2 nanotube arrays for photoelectrochemical determination of perfluorooctane sulfonate (PFOS). *Sens. Actuators B Chem.* **2014**, *190*, 745-751. DOI: https://doi.org/10.1016/j.snb.2013.09.048.
(97) León, M.; Silva, J.; Carrasco, S.; Barrientos, N. Design, Cost Estimation and Sensitivity Analysis for a Production Process of Activated Carbon from Waste Nutshells by Physical Activation. *Processes* **2020**, *8* (8), 945.
(98) Wong, S.; Ngadi, N.; Inuwa, I. M.; Hassan, O. Recent advances in applications of activated carbon from biowaste for wastewater treatment: A short review. *J. Clean. Prod.* **2018**, *175*, 361-375. DOI: https://doi.org/10.1016/j.jclepro.2017.12.059.
(99) Zhang, D.; Zhang, W.; Liang, Y. Adsorption of perfluoroalkyl and polyfluoroalkyl substances (PFASs) from aqueous solution-A review. *Sci. Total Environ.* **2019**, *694*, 133606.
(100) Ye, L. Synthetic Strategies in Molecular Imprinting. *Adv Biochem Eng Biotechnol* **2015**, *150*, 1-24. DOI: 10.1007/10_2015_313 From NLM.
(101) Deng, S.; Shuai, D.; Yu, Q.; Huang, J.; Yu, G. Selective sorption of perfluorooctane sulfonate on molecularly imprinted polymer adsorbents. *Front Environ Sci Eng China* **2009**, *3* (2), 171-177.
(102) Kasera, N.; Hall, S.; Kolar, P. Characterization data of N-doped biochars using different external nitrogen precursors. *J. Environ. Chem. Eng.* **2021**, *35*, 106870-106870. DOI: 10.1016/j.dib.2021.106870 PubMed.

(103) Liu, S.-H.; Huang, Y.-Y. Valorization of coffee grounds to biochar-derived adsorbents for CO2 adsorption. *J. Clean. Prod.* **2018**, *175*, 354-360. DOI: https://doi.org/10.1016/j.jclepro.2017.12.076.
(104) Maddi, C.; Bourquard, F.; Barnier, V.; Avila, J.; Asensio, M.-C.; Tite, T.; Donnet, C.; Garrelie, F. Nano-Architecture of nitrogen-doped graphene films synthesized from a solid CN source. *Scientific Reports* **2018**, *8* (1), 3247. DOI: 10.1038/s41598-018-21639-9.
(105) Chen, Z.; Li, C.; Gao, J.; Dong, H.; Chen, Y.; Wu, B.; Gu, C. Efficient Reductive Destruction of Perfluoroalkyl Substances under Self-Assembled Micelle Confinement. *Environ. Sci. Technol.* **2020**, *54* (8), 5178-5185. DOI: 10.1021/acs.est.9b06599 From NLM.
(106) Li, Y.-F.; Chien, W.-Y.; Liu, Y.-J.; Lee, Y.-C.; Lo, S.-L.; Hu, C.-Y. Perfluorooctanoic acid (PFOA) removal by flotation with cationic surfactants. *Chemosphere* **2021**, *266*, 128949. DOI: 10.1016/j.chemosphere.2020.128949.
(107) Ateia, M.; Arifuzzaman, M.; Pellizzeri, S.; Attia, M. F.; Tharayil, N.; Anker, J. N.; Karanfil, T. Cationic polymer for selective removal of GenX and short-chain PFAS from surface waters and wastewaters at ng/L levels. *Water Res.* **2019**, *163*, 114874. DOI: https://doi.org/10.1016/j.watres.2019.114874.
(108) Deng, S.; Zheng, Y. Q.; Xu, F. J.; Wang, B.; Huang, J.; Yu, G. Highly efficient sorption of perfluorooctane sulfonate and perfluorooctanoate on a quaternized cotton prepared by atom transfer radical polymerization. *Chem. Eng. J.* **2012**, *193-194*, 154-160. DOI: https://doi.org/10.1016/j.cej.2012.04.005.
(109) Teerlink, J.; Hernandez, J.; Budd, R. Fipronil washoff to municipal wastewater from dogs treated with spot-on products. *Sci. Total Environ.* **2017**, *599-600*, 960-966. DOI: https://doi.org/10.1016/j.scitotenv.2017.04.219.
(110) Lopez, J.; Monsalvo, V. M.; Puyol, D.; Mohedano, A. F.; Rodriguez, J. J. Low-temperature anaerobic treatment of low-strength pentachlorophenol-bearing wastewater. *Bioresour. Technol.* **2013**, *140*, 349-356. DOI: https://doi.org/10.1016/j.biortech.2013.04.049.
(111) Rigueto, C. V. T.; Nazari, M. T.; De Souza, C. F.; Cadore, J. S.; Brião, V. B.; Piccin, J. S. Alternative techniques for caffeine removal from wastewater: An overview of opportunities and challenges. *J. Water Process. Eng.* **2020**, *35*, 101231. DOI: https://doi.org/10.1016/j.jwpe.2020.101231.
(112) Millipore Sigma. *IR Spectrum Table and Chart*. Merck KGaA, 2022. https://www.sigmaaldrich.com/US/en/technical-documents/technical-article/analytical-chemistry/photometry-and-reflectometry/ir-spectrum-table (accessed 3/31/2022).
(113) Keiluweit, M.; Nico, P. S.; Johnson, M. G.; Kleber, M. Dynamic molecular structure of plant biomass-derived black carbon (biochar). *Environ. Sci. Technol.* **2010**, *44* (4), 1247-1253. DOI: 10.1021/es9031419.
(114) Kumarasamy, E.; Manning, I. M.; Collins, L. B.; Coronell, O.; Leibfarth, F. A. Ionic Fluorogels for Remediation of Per- and Polyfluorinated Alkyl Substances from Water. *ACS Cent. Sci.* **2020**, *6* (4), 487-492. DOI: 10.1021/acscentsci.9b01224.
(115) Quan, Q.; Wen, H.; Han, S.; Wang, Z.; Shao, Z.; Chen, M. Fluorous-Core Nanoparticle-Embedded Hydrogel Synthesized via Tandem Photo-Controlled Radical Polymerization: Facilitating the Separation of Perfluorinated Alkyl Substances from Water. *ACS Appl. Mater. Interfaces* **2020**, *12* (21), 24319-24327. DOI: 10.1021/acsami.0c04646.
(116) Belay, A.; Ture, K.; Redi, M.; Asfaw, A. Measurement of caffeine in coffee beans with UV/vis spectrometer. *Food Chem.* **2008**, *108* (1), 310-315. DOI: https://doi.org/10.1016/j.foodchem.2007.10.024.

(117) Vega, E.; Valdés, H. New evidence of the effect of the chemical structure of activated carbon on the activity to promote radical generation in an advanced oxidation process using hydrogen peroxide. *Micropor. Mesopor. Mat.* **2018**, *259*, 1-8. DOI: https://doi.org/10.1016/j.micromeso.2017.09.018.
(118) Zhuang, Q. L.; Kyotani, T.; Tomita, A. DRIFT and TK/TPD analyses of surface oxygen complexes formed during carbon gasification. *Energy Fuels* **1994**, *8* (3), 714-718. DOI: 10.1021/ef00045a028.
(119) Lath, S.; Knight, E. R.; Navarro, D. A.; Kookana, R. S.; McLaughlin, M. J. Sorption of PFOA onto different laboratory materials: filter membranes and centrifuge tubes. *Chemosphere* **2019**, *222*, 671-678. DOI: https://doi.org/10.1016/j.chemosphere.2019.01.096.
(120) Lei, Y.; Remmers, J. C.; Saakes, M.; van der Weijden, R. D.; Buisman, C. J. N. Is there a precipitation sequence in municipal wastewater induced by electrolysis? *Environ. Sci. Technol.* **2018**, *52* (15), 8399-8407. DOI: 10.1021/acs.est.8b02869 From NLM.
(121) USEPA. NPDES Writers Manual, Chapter 5: Technology Based Effluent Limitations. U.S. Environmental Protection Agency, Ed.; 2010.
(122) *Visual MINTEQ*; released 2014. (accessed.
(123) Wang, W.; Maimaiti, A.; Shi, H.; Wu, R.; Wang, R.; Li, Z.; Qi, D.; Yu, G.; Deng, S. Adsorption behavior and mechanism of emerging perfluoro-2-propoxypropanoic acid (GenX) on activated carbons and resins. *Chem. Eng. J.* **2019**, *364*, 132-138. DOI: https://doi.org/10.1016/j.cej.2019.01.153.
(124) Ray, J. R.; Wan, W.; Gilbert, B.; Jun, Y.-S. Effects of formation conditions on the physicochemical properties, aggregation, and phase transformation of iron oxide nanoparticles. *Langmuir* **2013**, *29* (4), 1069-1076. DOI: 10.1021/la3034319.
(125) Lawler, D. F.; Benjamin, M. M. *Water quality engineering : physical/chemical treatment processes*; Hoboken, New Jersey : John Wiley & Sons, 2013.